Software News and Update
MOLCAS 7: The Next Generation

FRANCESCO AQUILANTE,[1] LUCA DE VICO,[2] NICOLAS FERRÉ,[3] GIOVANNI GHIGO,[4] PER-ÅKE MALMQVIST,[5] PAVEL NEOGRÁDY,[6] THOMAS BONDO PEDERSEN,[5] MICHAL PITOŇÁK,[6,7] MARKUS REIHER,[8] BJÖRN O. ROOS,[5] LUIS SERRANO-ANDRÉS,[9] MIROSLAV URBAN,[6] VALERA VERYAZOV,[5] ROLAND LINDH[5]

[1]Department of Physical Chemistry, University of Geneva, 30 Quai Ernest Ansermet, CH-1211 Geneva, Switzerland

[2]Department of Chemistry, University of Copenhagen, Universitetsparken 5, DK-2100 Copenhagen, Denmark

[3]Chimie Théorique, Universités d'Aix-Marseille I,II,III-CNRS, UMR 6264 Laboratoire Chimie Provence, Faculté de Saint-Jérôme Case 521, Av. Esc. Normandie Niemen, 13397 Marseille Cedex 20, France

[4]Dipartimento di Chimica Generale e Chimica Organica, University of Turin, C.so M. d'Azeglio, 10125 Turin, Italy

[5]Department of Theoretical Chemistry, Chemical Center, P.O. Box 124, S-221 00 Lund, Sweden

[6]Department of Physical and Theoretical Chemistry, Faculty of Natural Sciences, Comenius University, Mlynska Dolina CH-1, 842 15 Bratislava, Slovak Republic

[7]Institute of Organic Chemistry and Biochemistry, Academy of Sciences of the Czech Republic and Center of Biomolecules and Complex Molecular Systems, Flemingovo nám. 2, 166 10 Prague 6, Czech Republic

[8] Laboratorium für Physikalische Chemie, ETH Zurich, Hönggerberg Campus, Wolfgang-Pauli-Strasse, 10, CH-8093 Zurich, Switzerland

[9]Departamento de Química Física, Instituto de Ciencia Molecular, Universitat de València, P.O. Box 22085, ES-46071 Valencia, Spain

Received 12 February 2009; Revised 3 April 2009; Accepted 6 April 2009
DOI 10.1002/jcc.21318
Published online 4 June 2009 in Wiley InterScience (www.interscience.wiley.com).

Abstract: Some of the new unique features of the MOLCAS quantum chemistry package version 7 are presented inthis report. In particular, the Cholesky decomposition method applied to some quantum chemical methods is described. This approach is used both in the context of a straight forward approximation of the two-electron integrals and in the generation of so-called auxiliary basis sets. The article describes how the method is implemented for most known wave functions models: self-consistent field, density functional theory, 2nd order perturbation theory, complete-active space self-consistent field multiconfigurational reference 2nd order perturbation theory, and coupled-cluster methods. The report further elaborates on the implementation of a restricted-active space self-consistent field reference function in conjunction with 2nd order perturbation theory. The average atomic natural orbital basis for relativistic calculations, covering the whole periodic table, are described and associated unique properties are demonstrated. Furthermore, the use of the arbitrary order Douglas-Kroll-Hess transformation for one-component relativistic calculations and its implementation are discussed. This section especially focuses on the implementation of the so-called picture-change-free atomic orbital property integrals. Moreover, the ElectroStatic Potential Fitted scheme, a version of a quantum mechanics/molecular mechanics hybrid

Correspondence to: R. Lindh; e-mail: roland.lindh@teokem.lu.se or V. Veryazov; e-mail: valera.veryazov@teokem.lu.se

Contract/grant sponsor: Swedish Science Research Council
Contract/grant sponsor: ETH Zurich; contract/grant number: ETH grant 0-20436-07
Contract/grant sponsor: Schweitzer Nationalfonds; contract/ grant number: project 200020-121870
Contract/grant sponsor: Slovak Research and Development Agency; contract/grant number: APVV-20-018405
Contract/grant sponsor: Ministry of Education of the Czech Republic (Center for Biomolecules and Complex Molecular Systems, LC512); contract/grant number: Z4 055 0506
Contract/grant sponsor: Consolider-Ingenio in Molecular Nanoscience of the Spanish MEC/FEDER; contract/grant numbers: CTQ2007-61260 and CSD2007-0010

method implemented in MOLCAS, is described and discussed. Finally, the report discusses the use of the MOLCAS package for advanced studies of photo chemical phenomena and the usefulness of the algorithms for constrained geometry optimization in MOLCAS in association with such studies.

 J Comput Chem 31: 224–247, 2010

Key words: MOLCAS; ANO-RCC; RASPT2; ESPF; Cholesky decomposition; coupled cluster; Douglas-Kroll-Hess; photo chemistry

Introduction

The origin of the MOLCAS* package can be traced back to the novel work during the 1970s of the group of Roos[1] at the Stockholm University, Sweden. Together with his students, J. Almöf, P. E. M. Siegbahn, and U. Wahlgren, they developed improved and novel methods for electron-integral evaluation (Molecule), the direct configuration interaction technique,[2] implemented single, and multiconfigurational reference configuration interaction (SDCI and MRCI),[3] developed the single most successful version of the multiconfigurational SCF method, the complete active space SCF (CASSCF) method,[4–6] derived new systematic Gaussian basis set for molecular calculation,[7–9] etc. Much of the work was inspired by the young scientist's visits to the quantum chemistry group at the IBM Almaden research center in San Jose, headed by E. Clementi. The work of the Stockholm group formed the backbone of the original version of MOLCAS, which was presented the first time in 1989. This, the first version of MOLCAS, had many similarities with the Molecule-Sweden package, which for many years was the work horse of the quantum chemistry group at NASA Ames. However, developments during the 1990 and the following decade has made MOLCAS into a more versatile and user-friendly program package as compared with the original version, which would only run on the IBM 3090 computers under the JCL operating system. Notable upgrades were the introduction of the multiconfigurational reference second order perturbation theory (CASPT2) approach[10–12] and the Multi-State CASPT2 (MS-CASPT2),[13] improved two-electron integral evaluation,[14,15] methods for gradient evaluation,[16,17] geometry optimization,[18,19] frequency calculations,[20] extensions to additional wave function methods, the generalization of the CASSCF to a restricted active space (RASSCF),[21,22] the development of the CASSCF state interaction method (CASSI),[23] the introduction of spin-orbit coupling (RASSI-SO),[24] and improvements with respect to single determinant methods, in particular it is worth to mention the work on coupled-cluster theory.[25] However, the MOLCAS package was for a long time a package which only targeted highly correlated calculations of rather small systems, although a DFT option has for some time been included. The status of the MOLCAS package, as of 2003, was at that time presented[26] and the philosophy and infrastructure behind the package was documented in a subsequent publication.[27]

*MOLCAS has derived its name from two of the modules in the original version, the Molecule integral generator of J. Almlöf and the CASSCF module of B. O. Roos. Neither the Molecule nor the CASSCF module made their way to the second version of MOLCAS, in which they were replaced with more general substitutes. http://www.molcas.org

MOLCAS version 7, as compared with earlier versions, constitutes a substantial improvement regarding the size of the systems which can be handled by the various wave function models, the versatility of the package, the applicability of the implemented methods to the whole periodic table, improvements with respect to the bottleneck within the CASSCF/CASPT2 paradigm—the size of the so-called active space—implementation of a quantum mechanics/molecular mechanics (QM/MM) model which can in principle support any kind of MM force-fields and the applicability of the package to significant parts of the lower excited states as, for example, expressed by photochemistry. This report here will present these new developments and extensions in a compact and easy-to-understand way. The purpose of the article, however, is not to be too detailed, but to summarize the methods and implementation into a single document. It should be mentioned that the newest version of MOLCAS does not only include these reported new features. Additional improvements as a simplified user input, a graphical user interface, add-ons, improved tutorials, etc., are not included in this report. Furthermore, some of the methods presented here relates to parallelization. In that respect it should be noted that the RASSCF and RASPT2 modules only include parallelization with respect to the formation of Fock-matrices and transformed two-electron repulsion integrals.

Cholesky Decomposition in MOLCAS

Storage and transformation of two-electron integrals from atomic orbital (AO) to molecular orbital (MO) basis have been major bottlenecks in previous versions of MOLCAS. As of version 7, however, MOLCAS features the Cholesky decomposition (CD) technique[28,29] which substantially reduces the effort involved in two-electron integral handling.[30–32] The CD is also used for generating auxiliary basis sets for the density fitting (DF)/resolution-of-the-identity (RI) technique,[33–38] which is available in MOLCAS-7 as well.[39] The CD-based development in MOLCAS-7 has been published in a number of research papers[39–47] and a review will appear soon (Pedersen et al., Theor Chem Acc, to be submitted).

Cholesky Decomposition of Two-Electron Integrals

The Cholesky representation of the two-electron integrals in AO basis is given by[30,31]

$$(\mu\nu|\lambda\sigma) \approx \sum_{J=1}^{M} L^J_{\mu\nu} L^J_{\lambda\sigma}, \tag{1}$$

where we have used Mulliken notation for the integrals and Greek letters to denote AOs. The Cholesky vectors are computed from a residual matrix in a recursive procedure according to

$$L^J_{\mu\nu} = \left[\Delta^{(J-1)}_{[\lambda\sigma]_J,[\lambda\sigma]_J}\right]^{-1/2} \Delta^{(J-1)}_{\mu\nu,[\lambda\sigma]_J}, \tag{2}$$

where the residual matrix is defined by

$$\Delta^{(J)}_{\mu\nu,\lambda\sigma} = (\mu\nu|\lambda\sigma) - \sum_{K=1}^{J} L^K_{\mu\nu} L^K_{\lambda\sigma}, \tag{3}$$

and $[\lambda\sigma]_J$ is the index of the largest residual diagonal element at the $(J-1)$th recursion, i.e., the index of the parent product $|\lambda\sigma)$ giving rise to the Jth Cholesky vector. We refer to the subset $\{|[\lambda\sigma]_J)\}$ of the product functions as the Cholesky basis.

A symmetric positive semidefinite matrix,[30] the residual matrix satisfies the Cauchy-Schwarz inequality

$$\left|\Delta^{(J)}_{\mu\nu,\lambda\sigma}\right| \le \sqrt{\Delta^{(J)}_{\mu\nu,\mu\nu}\Delta^{(J)}_{\lambda\sigma,\lambda\sigma}}. \tag{4}$$

Introducing the decomposition threshold $\delta \ge 0$ and using

$$\max_{\mu\nu}\left(\Delta^{(M)}_{\mu\nu,\mu\nu}\right) \le \delta, \tag{5}$$

as stop criterion for the recursive procedure, we obtain from eq. (4) that the integrals are represented with absolute accuracy δ:

$$\left|\Delta^{(M)}_{\mu\nu,\lambda\sigma}\right| \le \delta. \tag{6}$$

It should be noted, however, that the subset of the integrals corresponding to the parent product functions is represented exactly (within machine precision):

$$\Delta^{(M)}_{[\mu\nu]_J,[\lambda\sigma]_K} = 0. \tag{7}$$

This means that the "most important" (as defined by the CD procedure) integrals are represented exactly and is a fundamental reason why the CD technique is accurate even with rather large values of the decomposition threshold.[47]

The computational bottleneck of the CD procedure is the calculation of the residual matrix, eq. (3). In an integral-direct approach,[31] only those columns that give rise to Cholesky vectors are calculated, meaning that only a fraction (usually 1–5%) of the integral matrix is needed to generate the Cholesky representation. Calculation of the residual matrix requires two steps in each recursion: calculation of the integral column $(\mu\nu|[\lambda\sigma]_J)$ and subtraction of contributions from previous Cholesky vectors. Which of the two steps is the more expensive depends on the nature of the basis functions (number of primitive Gaussians, angular quantum number) and on the value chosen for the decomposition threshold. For basis sets with a large number of primitive Gaussians and with high angular quantum numbers, the integral calculation step tends to dominate, whereas the subtraction step usually dominates for smaller basis sets. The subtraction shows a computational complexity of $N_p M^2$ where N_p is the number of significant product functions $|\mu\nu)$, as estimated using the Cauchy-Schwarz inequality. Decreasing the decomposition threshold (increasing accuracy) therefore leads to a computational penalty scaling quadratically with the increase of the number of Cholesky vectors. The Cholesky vectors are stored in a buffer in memory. When the buffer is full, the vectors must be read back into memory from disk, creating a potential I/O bottleneck which can be reduced or avoided by increasing memory.

Damped prescreening based on eq. (4) is employed in each recursion. Specifically, a product function $|\mu\nu)$ is removed when the following inequality is satisfied:

$$s\sqrt{\Delta^{(J)}_{\mu\nu,\mu\nu}\Delta^{(J)}_{\max}} \le \delta, \tag{8}$$

where $\Delta^{(J)}_{\max}$ is the largest residual diagonal and $s \ge 1$ is the damping. The latter is chosen according to $s \approx 10^9\delta$ for decomposition thresholds above 10^{-8} and $s = 1.0$ for lower thresholds. As a consequence of the damped prescreening, the dimension of the Cholesky vectors is decreased in each recursion and even integrals with values below the decomposition threshold have a nonzero Cholesky representation. As noted in ref. 31, the damping serves as a safeguard against rounding errors that may render the decomposition numerically unstable.

SEWARD, the integral program of MOLCAS, is atomic shell-driven.[14] As a consequence, individual integral columns cannot be efficiently calculated, and we compute instead the entire set of integral columns $(\mu\nu|AB)$ where AB denotes the shell-pair to which the largest residual diagonal element belongs. New Cholesky vectors are then generated from this shell-pair as long as the largest residual diagonal element within this shell-pair is at least a "span factor" times the globally largest residual diagonal element. The default span factor in MOLCAS is 0.01, meaning that the CD recursions continue within the calculated shell-pair until the globally largest diagonal is more than 100 times larger. This shell-driven integral-direct approach has two consequences: first, the total number of Cholesky vectors depends weakly on the chosen span factor and, second, shell-pair integral columns may be calculated more than once. The latter is, of course, particularly important for large basis sets where the integral calculations are expensive.

To reduce the cost of integral recalculations, the decomposition is performed in two steps. In the first step, all rows and columns of the residual matrix corresponding to diagonal elements smaller than the decomposition threshold are discarded in each recursion. In other words, all diagonals that cannot give rise to a Cholesky vector are removed, minimizing the dimension of the residual matrix to be calculated in each recursion. The computational cost of integral recalculations and Cholesky vector I/O is thus minimized due to the low dimension of the residual matrix. The essential output from the first step is the Cholesky basis, i.e., the mapping from the vector index J to the parent product index $\lambda\sigma$. Given this mapping, the full-dimension Cholesky vectors are calculated in the second step according to eq. (2) with the prescreening of eq. (8). Integral recalculations are thus avoided and Cholesky vector I/O minimized in the second step.

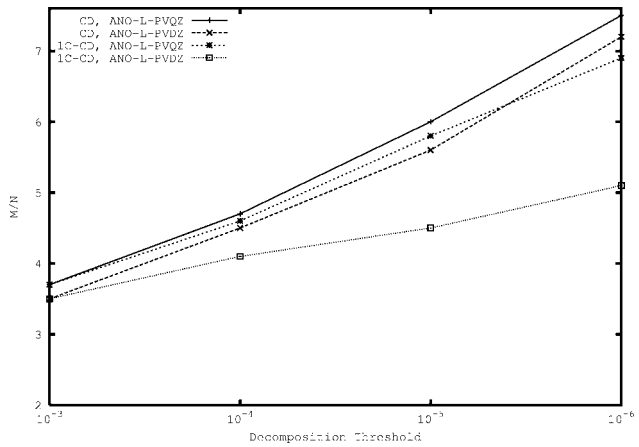

Figure 1. The ratio M/N as a function of decomposition threshold for ANO-L-PVXZ ($X = D, Q$) AO basis sets. M is the number of Cholesky vectors and N the number of AO basis functions. The ratio is calculated as an average for the molecules of Set I (a subset of the G2-97 test set) of ref. 47.

In a parallel execution, the rows of the residual matrix are (statically) distributed among the processes. In a given recursion, each process calculates the corresponding rows of the integral matrix and performs the subtraction of previous Cholesky vectors according to eq. (3). This requires that the Cholesky vector elements corresponding to the selected integral columns [$L^K_{\lambda\sigma}$ in eq. (3)] are broadcast from the process holding them. This design ensures that the memory requirement per process is minimized and that Cholesky vector I/O can be avoided by increasing the number of compute nodes (increasing available memory). Once the CD has completed, the Cholesky vectors are stored on disk for later use. For the disk storage, however, complete Cholesky vectors are distributed among the nodes, i.e., $\mathbf{L}^1$ is stored on node 0, $\mathbf{L}^2$ on node 1, $\mathbf{L}^3$ on node 2, and so on.

The Cholesky basis generally contains both one- and two-center product functions. We have implemented the so-called one-center CD (1C-CD)[39] in which no two-center functions are allowed to enter the Cholesky basis. As shown in ref. 47, the two-center functions are needed for high accuracy (low decomposition threshold), in particular with lower-quality AO basis sets. As can be seen in Figure 1, the computational advantage (lower M) of 1C-CD increases with decomposition threshold and is particularly pronounced for the double-ζ (lower quality) basis set. The scaling of M with system size is linear, as seen from Figure 2. As the scaling of the number of AO basis functions, N, is trivially linear, this implies that the ratio M/N is constant, as also shown in Figure 2.

Analytic gradients of the integrals have been defined for the Cholesky representation.[43] At the moment, however, analytic gradients can only be calculated in conjunction with nonhybrid DFT and the 1C-CD option. Numerical gradients can be calculated with all CD-based options, of course.

Quantum Chemistry with Cholesky Decomposition

Having performed the CD of the two-electron integral matrix, the resulting Cholesky vectors can be used for HF, DFT, MP2, scaled opposite spin (SOS) MP2, RASSCF, CASSCF, RASSI, CASPT2, and CCSD(T) calculations. The Cholesky vectors are used directly to construct Fock matrices and two-electron integrals in MO basis.

Inactive and active Fock matrices are calculated in AO basis according to[41,44]

$$F_{\mu\nu} = \sum_J L^J_{\mu\nu} \sum_{\lambda\sigma} L^J_{\lambda\sigma} D_{\lambda\sigma} - \frac{1}{2} \sum_J \sum_k L^J_{\mu k} L^J_{\nu k}, \tag{9}$$

where k runs over either inactive or active orbital indices and $\mathbf{D}$ is the corresponding density matrix. The half-transformed Cholesky vectors are calculated according to

$$L^J_{\mu k} = \sum_\nu L^J_{\mu\nu} C_{\nu k}, \tag{10}$$

where $\mathbf{C}$ is the MO coefficient matrix. Although the Coulomb part of eq. (9) scales quadratically with system size, the exchange part, including the transformation of eq. (10), scales cubically. We have therefore developed the "Local Exchange" (LK)[39] algorithm, which reduces the scaling to quadratic by using localized MOs and prescreening based on rigorous upper bounds. To reduce the computational cost of orbital localization, MOLCAS uses the so-called Cholesky MOs obtained by performing a CD of the density matrix.[40]

Two-electron integrals in MO basis are calculated from transformed Cholesky vectors according to

$$(pq|rs) = \sum_J L^J_{pq} L^J_{rs}, \tag{11}$$

where p, q, r, s denote MOs, and

$$L^J_{pq} = \sum_\mu C_{\mu p} \sum_\nu L^J_{\mu\nu} C_{\nu q}. \tag{12}$$

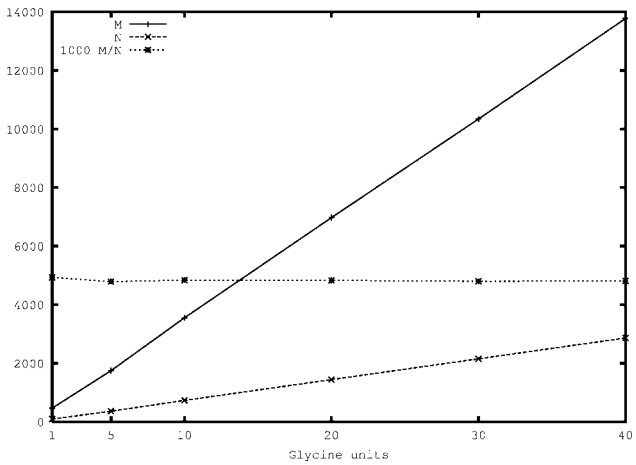

Figure 2. The number of Cholesky vectors M, number of AO basis functions N, and the ratio M/N (multiplied by 1000) as functions of the number of glycine units in linear glycine chains. The basis set is cc-pVDZ and the decomposition threshold is $\delta = 10^{-4}$.

Only those integrals that are needed by a given method are computed according to eq. (11), thus significantly reducing the computational cost compared with conventional calculations. MOLCAS generates the $(ai|bj)$ integrals on-the-fly while calculating the MP2 energy correction [i, j refer to occupied orbitals, a, b to virtual orbitals], whereas the MO integrals needed by the CASPT2 method are generated, written to disk, and read back into memory in the CD-CASPT2 implementation. Although the CD-MP2 code is significantly faster than the conventional implementation, the CD-CASPT2 code mainly reduces the wall-time of the calculation due to decreased I/O.[45] Both CD-MP2 and CD-CASPT2 can be applied to substantially larger systems than the conventional programs, as exemplified in refs. 45, 48, 49. As described in more detail below, the new CD-based implementation of coupled cluster theory in MOLCAS can use Cholesky vectors in two ways. Either the MO integrals are calculated and stored on disk prior to the iterative CCSD procedure or they are calculated on-the-fly.

Density Fitting and Auxiliary Basis Sets from Cholesky Decompositions

The DF approximation is given by[33–38]

$$(\mu\nu|\lambda\sigma) \approx \sum_{PQ} (\mu\nu|P) G^{-1}_{PQ} (\lambda\sigma|Q), \tag{13}$$

where P, Q refer to auxiliary basis functions, $G^{-1}_{PQ} = (\mathbf{G}^{-1})_{PQ}$, and $G_{PQ} = (P|Q)$. As the $\mathbf{G}$ matrix is symmetric positive definite, its inverse can be Cholesky decomposed, i.e.

$$G^{-1}_{PQ} = \sum_{K} Z^K_P Z^K_Q. \tag{14}$$

Combining eq. (14) and eq. (13), and introducing the DF vectors

$$R^K_{\mu\nu} = \sum_{P} (\mu\nu|P) Z^K_P, \tag{15}$$

we obtain the expression

$$(\mu\nu|\lambda\sigma) \approx \sum_{K} R^K_{\mu\nu} R^K_{\lambda\sigma}, \tag{16}$$

which has the same form as the Cholesky representation, eq. (1). The DF vectors are generated by SEWARD and stored in the same manner as Cholesky vectors. Thus, the MOLCAS modules using Cholesky vectors can also be executed using DF vectors.

MOLCAS generates auxiliary basis sets on-the-fly, as described in refs. 39, 46 and benchmarked along with CD in ref. 47. Two types of CD-based auxiliary basis sets are available in MOLCAS: the atomic CD (aCD)[39] and the atomic compact CD (acCD).[46] The aCD set is generated by a decomposition of the atomic two-electron integral matrix, identifying the resulting Cholesky basis (see above) as the auxiliary functions for the given atom type and basis set. To make the integral evaluation more efficient, "missing" angular components of the product functions of the Cholesky basis are added to complete the shell structure of the auxiliary basis (see refs. 39, 46 for further details). The acCD set is generated from the corresponding aCD set by removing linear dependence in the primitive Gaussian product basis by performing a CD of an "angular free" integral matrix, as described in ref. 46. The number of auxiliary functions is thus the same for aCD and acCD sets, but the number of primitive Gaussians is reduced in the latter, making the generation of DF vectors faster for large basis sets. The accuracies of the aCD and acCD sets are almost identical, though.[46,47]

As the aCD and acCD auxiliary basis sets are constructed by CD of the atomic integral matrix, they may be used with any AO basis set. Moreover, they may be used in conjunction with any quantum chemical method. In short, the aCD and acCD auxiliary basis sets are unbiased. Constructed on-the-fly, the aCD and acCD basis sets are generated automatically in MOLCAS, requiring no other user-input than the decomposition threshold (if the default is not sufficient). Care must be exercised for small AO basis sets on hydrogen and helium atoms; however, in the absence of polarization functions in the AO basis set, the aCD and acCD sets solely contain s-functions on hydrogen and helium atoms, leading to unusually large errors in total energies.[46]

ANO-RCC: A Basis Set for the Entire Periodic Table

MOLCAS is a program system that allows calculations in the relativistic regime. As described earlier, the Douglas-Kroll-Hess (DKH) transformation of the Dirac Hamiltonian is used in a two-component formulation of the relativistic wave function. The scalar part of the DKH Hamiltonian replaces the one-electron nonrelativistic Hamiltonian and all methods that are used in nonrelativistic calculations will automatically include these effects. However, the basis sets that are normally used cannot be transferred to the relativistic regime. The contraction of the inner shells are different and this will affect the structure also for the valence orbitals. It is therefore necessary to develop specific basis sets where the DKH Hamiltonian is included when the basis set is constructed.

Here we have developed such basis sets for the atoms H-Cm based on the concept of density averaged Atomic Natural Orbitals (ANOs). Such basis sets have been available in MOLCAS in the nonrelativistic regime for the atoms H-Zn, as the ANO-L and ANO-S basis sets.[50–53] The new basis sets have been labelled ANO-RCC to indicate that they are relativistic (R) and that semicore electrons have been included in the correlation treatment (CC). The densities used for the construction of the ANOs have been obtained from multiconfigurational wave functions have been used (CASSCF) with the most important orbitals in the active space, where dynamic correlation is treated using second order perturbation theory (CASPT2).[10,11,54] This approach was used because it is general and can be applied to all electronic states independent of their spin and space symmetry. The basis sets have been generated without the inclusion of spin-orbit coupling which we do not believe to be very important for the shape of the orbitals (with the exception of the heavier main group elements, where the present approach will not work well anyway). The ANO-RCC basis sets have been published in a series of papers during the years 2003–2008.[55–59]

Table 1. Size of the Primitive Basis Sets and the Contraction Range.

Atoms	Primitive	Max # of ANOs	Atoms	Primitive	Max # of ANOs
H	8s4p3d1f	6s4p3d1f	Rb–Sr	23s19p11d4f	10s10p5d4f
He	9s4p3d2f	7s4p3d2f	Y–Cd	21s18p13d6f4g2h	10s9p8d5f4g2h
Li–Be	14s9p4d3f1g	8s7p4d2f1g	In–Xe	22s19p13d5f3g	10s9p8d5f3g
Be–Ne	14s9p4d3f1g	8s7p4d3f2g	Cs–Ba	26s22p15d4f	12s10p8d4f
Na	17s12p5d4f	9s8p5d2f	La	24s21p15d5f3g	11s10p8d5f3g
Mg	17s12p6d2f	9s8p6d2f	Ce–Lu	25s22p15d11f4g2h	12s11p8d7f4g2h
Al	17s12p5d3f	9s9p5d3f	Hf–Au	24s21p15d11f4g2h	11s10p8d6f4g2h
Si–Ar	17s12p5d4f2g	8s7p5d4f2g	Hg	25s22p16d12f4g2h	10s10p9d6f4g2h
K	21s16p5d4f	10s9p5d3f	Tl–Rn	25s22p16d12f4g	11s10p9d6f4g
Ca	20s16p6d4f	10s9p6d4f	Fr–Ra	28s25p17d12f	12s11p8d5f
Sc–Zn	21s15p10d6f4g2h	10s9p8d6f4g2h	Ac–Pa	27s24p18d14f6g3h	13s11p10d8f6g3h
Ga–Kr	20s17p11d5f2g	9s8p6d4f2g	U–Cm	26s23p17d13f5g3h	12s10p9d7f5g3h

The Average Densities

The primitive Gaussian functions used to construct the basis sets are presented in Table 1. For atoms up to Zn the ANO-L primitives were used. The primitives for the other atoms were based on the Faegri primitive sets.[60] They were extended with more diffuse functions in an even-tempered way. Higher angular momentum functions were added and exponents were optimized for the ground state atoms (at the CASPT2 level of theory) using an even-tempered extension with a ratio of 0.4.

The construction of the ANOs is based on an average density matrix. Calculations with the primitive basis set were performed for: each atom in its ground state, in one excited state, for the positive ion, and for most atoms also the negative atom. Polarization effects were included by calculations on the ground state atom in an electric field. For the main group elements calculations were instead made for the diatomic molecule. More details about the selected electronic states can be found in the original articles.[55–59] An average density matrix was constructed as:

$$\rho_{av} = \sum_i \omega_i \rho_i, \tag{17}$$

where ρ_i are the density matrices obtained from the different CASPT2 wave functions. Usually, the same weight was used for all states included in the averaging. The average density matrix is diagonalized and ANOs with occupation numbers larger than about 10^{-6} define maximum size of the basis set. For more details, we refer to the basis set library in the MOLCAS package.

Atomic Ionization Energies, Electron Affinities, and Polarizabilities

As examples of results that have been obtained during the construction of the basis set we present below the ionization energies(IEs) of all atoms in the range H-Cm, selected electron affinities, and polarizabilities for spherical atoms. The IEs are shown in Figure 3. Calculations have been performed with the largest basis set but almost identical results are obtained at the VQZP level. These CASPT2 results have an RMS error of 0.15 eV and a maximum error of 0.28 eV (for the Tc atom). The errors are mainly due to the CASPT2 approximation and to a lesser extent to limitations in the basis set.

Electron affinities (EAs) were computed for atoms for which positive values have been reported in Handbook in Chemistry and Physics.[62] They are presented in Figure 4. The RMS error is 0.17 eV and the maximum error is 0.40 eV (for the Fe atom). The RMS error would have been smaller if it was not for a few atoms where the difficulties in computing the EA were especially large. Most striking is the Fe atom with a measured EA of 0.15 eV. The computed value was −0.25 eV. The negative value was obtained by forcing the negative ion to have the electronic configuration d^7s^2 with all $3d$ orbitals equal. The larger errors naturally occur for atoms with small EAs where more diffuse functions are needed for an accurate description of the electronic structure of the negative ion. For the same reason, the computed EAs in almost all cases are smaller than experiment.

Finally, we show in Figure 5 the computed polarizabilities for the spherical atoms. They have been obtained using finite field perturbation theory at the CASPT2 level of theory. The basisset is clearly adequate for this purpose. All computed values are within

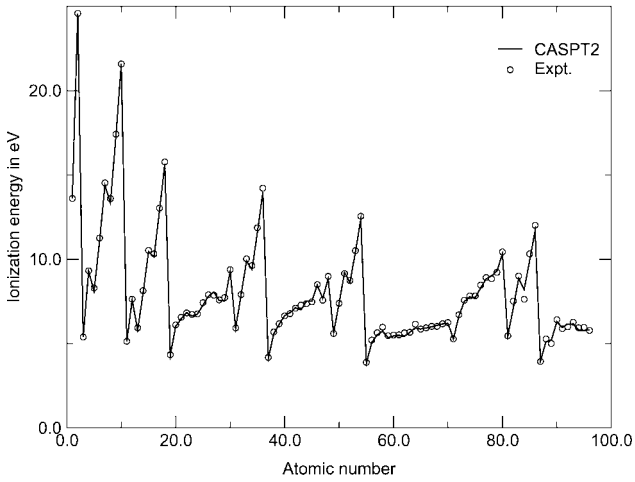

Figure 3. Ionization energies for the atoms H-Cm (in eV). Experimental values from ref. 61.

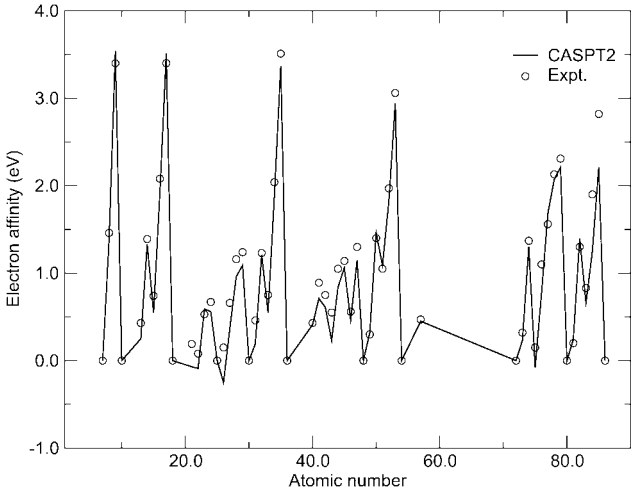

Figure 4. Electron affinities for some selected atoms (in eV). Experimental values from ref. 62.

the error limits of experiment.[62] More information about the performance of the ANO-RCC basis sets can be found in the basis set library (www.molcas.org) from where these basis sets can also be downloaded.

Relativistic Douglas-Kroll-Hess Energies and Properties

The nonrelativistic electronic Schrödinger equation provides only an approximate description of reality, which is only valid in those cases where the speed of the electrons is small compared to the speed of light. As a consequence, standard Schrödinger quantum mechanics is only sufficiently accurate for molecules containing atoms with small nuclear charges like carbon or oxygen in which the electrons do not acquire a speed that approaches a significant portion of the speed of light. In chemistry, a quantum mechanical model theory is sought valid for the full periodic table of the elements. In principle, this is accomplished by a first-quantized many-electron theory based on Dirac's theory of the electron.[63]

In this so-called four-component theory, the one-electron part of the Fock operator is given by the Dirac Hamiltonian,

$$h_{\mathrm{D}} = c\boldsymbol{\alpha}\cdot\boldsymbol{p} + (\beta - \mathbf{1}_4)mc^2 + V, \qquad (18)$$

which has been shifted by the rest energy $mc^2\mathbf{1}_4$ to match the nonrelativistic energy scale. The three components of the vector $\boldsymbol{\alpha}$ contain the three Pauli spin matrices on the off-diagonal positions. The diagonal matrices $\mathbf{1}_4$ and β contain the entries $(1, 1, 1, 1)$ and $(1, 1, -1, -1)$, respectively. As usual, $\boldsymbol{p}$ represents the momentum operator and c and m denote the speed of light and the rest mass of the electron, respectively. The potential V is simply given by the instantaneous electron–nucleus Coulomb interaction if we neglect the interaction of the electrons and if magnetic and retardation contributions are not taken into account. Because of the (4×4)-structure of the Dirac Hamiltonian, the molecular orbitals become four-component molecular spinors. Compared with one-component Schrödinger-based orbitals, these 4-spinors require quite some alteration of the algorithmic structure of a one-component quantum chemistry program apart from the fact that the computational effort increases. It is therefore desirable to find a representation of relativistic one-electron Hamiltonians which are sufficiently accurate and easy to interface with efficient one-component quantum chemical methods.

A large body of numerical evidence demonstrated that quasi-relativistic Hamiltonians in combination with multiconfiguration wave-function approximations yields an efficient method of sufficient overall accuracy for chemical purposes.[64–66]

The quasi-relativistic Hamiltonian employed according to this MOLCAS philosophy of consistent accuracy comprises the important kinematic contribution covered by the scalar-relativistic Douglas–Kroll–Hess (DKH) Hamiltonian[67,68] as well as efficient treatments of spin–orbit coupling via the atomic mean-field integral method and perturbation theory.[24]

The central idea of the DKH unitary transformation technique is to block-diagonalize the Dirac Hamiltonian h_{D} by a suitably chosen unitary transformation U

$$h_{\mathrm{bd}} = Uh_{\mathrm{D}}U^{\dagger} = \begin{pmatrix} h_+ & 0 \\ 0 & h_- \end{pmatrix} = \sum_{k=0}^{\infty} \begin{pmatrix} \mathcal{E}_k^{(+)} & 0 \\ 0 & \mathcal{E}_k^{(-)} \end{pmatrix}, \qquad (19)$$

to eliminate the small components of the molecular 4-spinors which would otherwise give rise to the unwanted negative-energy (often called positronic) states. The electronic bound and continuum states are completely described by the operator h_+, which can be decomposed into $\mathcal{E}_k^{(+)}$ operators featuring a well-defined order k in the external potential V.

In DKH theory, the unitary transformation U is decomposed into a sequence of transformations $\ldots U_2U_1U_0$, which produces the $\mathcal{E}_k^{(+)}$ step by step. An expansion in terms of the formal parameter $1/c$, which is identical to the fine-structure constant in atomic units, is ill-defined[69] and yields singular operators like the Pauli Hamiltonian, which is valid only in perturbation-theory treatments

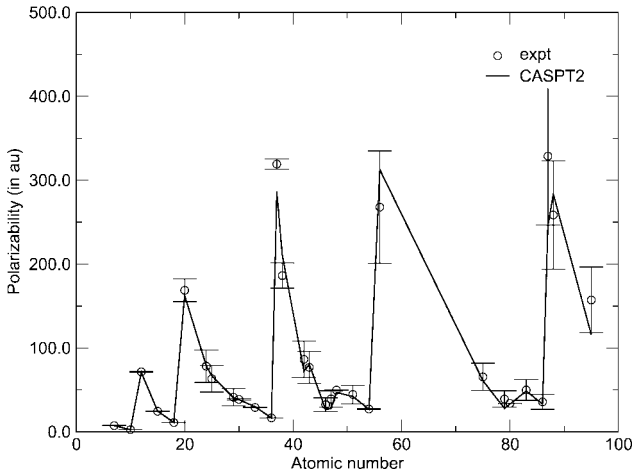

Figure 5. CASPT2 polarizabilities for the spherical atoms. Experimental values from ref. 62.

of relativistic effects. The expansion of h_{bd}, using the external potential V as perturbation parameter, does not give singular operators and can be used variationally.[69] The well-known relativistic terms of the Pauli Hamiltonian, like the mass–velocity and Darwin operators, are recovered from the DKH Hamiltonian after $1/c$ expansion. Hence, the variationally stable DKH Hamiltonians are an ideal substitute for the Pauli Hamiltonian and its ingredients, which are now only of historical importance.

Except for the first unitary transformation U_0, which must be chosen to be the free-particle Foldy–Wouthuysen transformation,[69] each unitary transformation U_i can be parameterized in terms of an anti-Hermitian operator to be chosen in such a way as to eliminate the off-diagonal coupling terms in the Dirac Hamiltonian. This parameterization can be written in terms of a Taylor series expansion in the most general fashion.[70] In actual calculations, a set of coefficients needs to be chosen for this expansion under the condition that unitarity is still preserved. Up to fourth order in V, the resulting Hamiltonians are independent of this choice, whereas higher-order Hamiltonians are affected by the choice of parameters. This parameter dependence is, however, negligible[71] and vanishes, of course, at infinite order. The arbitrary-order DKH method[72] has been implemented in its scalar-relativistic one-electron variant in the MOLCAS program package. A conceptual review of the method can be found in ref. 73. Five different parameterizations are available in MOLCAS, namely, the optimum, the square-root, the Cayley, the McWeeny, and the exponential parameterizations.

The unitary transformation technique that is at the heart of DKH theory requires not only the Hamiltonian to be unitary-transformed but any operator $\hat{o}$. For a sum of one-electron operators this reads

$$\langle \hat{o} \rangle = \sum_{ij} \gamma_{ij} \langle \psi_i^{\mathrm{DKH}} | \left(U \hat{o} U^{\dagger} \right) | \psi_j^{\mathrm{DKH}} \rangle, \qquad (20)$$

where ψ_i^{DKH} denotes the DKH orbitals and γ_{ij} is a generalized occupation number (i.e., an element of the first-order density matrix to be more precise). If this change of picture is not consistently considered, numerical artifacts appear in molecular property calculations that are called picture-change errors.[74,75] These artifacts can be reduced to any desirable order in DKH theory[76] and an arbitrary-order algorithm[77] has been implemented into the MOLCAS program package.[78]

It is an interesting feature of magnetic-field-free scalar-relativistic one-electron DKH theory that the resulting DKH Hamiltonian and DKH property operators can be calculated almost solely from the nonrelativistic integral matrices. Only two additional types of one-electron integral matrices are required, namely, $\{\langle \chi_\mu | \boldsymbol{p} \cdot V \boldsymbol{p} | \chi_\nu \rangle\}$ and $\{\langle \chi_\mu | \boldsymbol{p} \cdot \hat{o} \boldsymbol{p} | \chi_\nu \rangle\}$, where χ_μ and χ_ν are the usual atom-centered Gaussians. The transformation would, however, be more complicated for magnetic-field-dependent properties and for properties that require the perturbed wave function.[79]

Currently, all one-electron electric-field-like molecular property integrals are subject to a DKH transformation if this is switched on for the one-electron part of the Fock operator. The efficiency of the implementation has been demonstrated for electric-field gradients,[78] which are most prone to picture-change artifacts compared with other electric-field-like properties.[77] It is important to note that for every physical observable the change of picture must be taken into account. This is also true for the DKH density,[80] which cannot be simply obtained by adding squared DKH orbitals. For instance, the present implementation in MOLCAS allows one to calculate accurate parameters relevant to Mössbauer spectroscopy.[81] To demonstrate the convergence properties of the DKH series, we present in Figure 6 data for the principal component of the diagonalized electric field gradient tensor evaluated at the At nucleus in HAt from ref. 80.

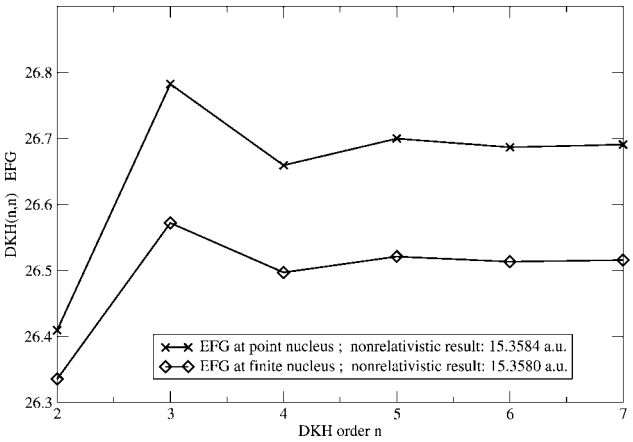

Figure 6. Principal component of the diagonalized electric field gradient tensor EFG in HAt (in a.u.) obtained at the At nucleus from high-order DKH(n, n) calculations with $n = 2, \ldots, 7$ according to data presented in ref. 80 The results depend on whether the At nucleus is assumed to be finite or point-like. Note the characteristic oscillating convergence behavior of the DKH series. The legend contains the nonrelativistic result given for comparison.

The RASPT2 Method

Nondynamic and Dynamic Correlation

Quantitative results by *ab initio* quantum mechanical methods requires a more or less accurate description of the electronic correlation. In many cases, e.g., for structure optimization, this can be achieved by a Kohn-Sham density functional method, DFT, using a correlation energy density parametrized as a local function of variables such as the electronic density, spin density, and their gradients. Such methods differ by the choice of this function, and while they have the merit of a computational complexity of similar order as Hartree-Fock, or even less if the Hartree-Fock exchange does not have to be computed, DFT methods remain unreliable or useless when this function is not accurate enough. For higher accuracy, the Coupled Cluster method with perturbative triples, CCSD(T), is the usual choice, but can be too expensive in terms of computer time. The cheaper perturbative second order Møller-Plesset method, MP2, can be used and may, or may not, be better than DFT, depending on application and choice of DFT functional.

The above methods will fail when multiconfigurational effects are of importance or when the calculations should treat with similar accuracy a variety of electronic structures. The multiplet states of transition metals give rise to a multitude of interacting configurations when they are involved in bonding. Multiple bonds usually

have a component, such as π bonds of most molecules or δ bonds between transition metals, which has fractional character. Excited states almost always involve several different electronic configurations, and for photochemistry the most interesting reaction paths are often those which pass through regions of swift changes of the adiabatic electronic states.

Traditionally, the correlation effects are classified as dynamic or nondynamic correlation. This classification is by no means strict, nor is it additive. The nondynamic correlation can be stabilizing or destabilizing, depending on the state. It describes a global electronic structure that cannot be properly modelled by a single-determinant wave function. The dynamic correlation, on the other hand, is regarded as resulting mainly from the additional stabilization by the ability of electrons to simultaneously avoid each other, with small and local effects in the electronic structure. In such a view, the dynamic correlation is always stabilizing.

A method that allows a flexible description of non-dynamic correlation is the Complete Active Space Self-Consistent Field (CASSCF) method. It is well suited for dealing with nondynamic near-degeneracy effects, thereby being able to treat electronically excited molecules, bond dissociation, radicals, transition metal compounds, etc., in the same way and with almost uniform accuracy. The CASSCF method is in principle open-ended, in the sense that a more accurate calculation can always be obtained by increasing the number of correlated orbitals. However, the number of configurations can grow dramatically with such an increase, and for molecules it is not possible to include more than a fraction of dynamic correlation in this way (In fact, the CASSCF model often serves as the operational definition of nondynamic correlation). New approaches, whereby in effect very large CI expansions can be used without the need for explicit representation of each individual CI coefficient,[82–84] offer a possible way to allow larger active spaces, but these are still experimental and it is probable that the dynamic correlation must still be treated by separate calculations.

Dynamic correlation effects "on top" of CASSCF, and including its interplay with the non-dynamic correlation, using, e.g., DFT or Coupled-Cluster methods, is either not technically possible or are still impractical for large molecular systems, even if there are development under way in this direction. On the other hand, the MP2 method has been extended such that it can compute a perturbative correction to CASSCF. This has been implemented as so-called CASPT2 (CAS Perturbation Theory through second order), and the combination CASSCF/CASPT2 has turned out to be very successful for a large variety of problems. There are also other approaches to such corrections. Celani et al.[85] made a very large calculation of the Cr_2 bonding using a combined CI/PT2 approach, and compare with CASPT2 and with another perturbation scheme, called NEVPT2.[86]

The combination of CASSCF and CASPT2 is almost always necessary, as CASSCF alone has very limited ability to handle dynamic correlation. Once that the CASSCF has taken care of nondynamic correlation, the remaining dynamic correlation is much easier to deal with. It is still large and variable enough that it must usually be included, but can be treated perturbatively.

The CASSCF/CASPT2 method is quite complicated in its details and implementation, but it has now reached a mature state and has been shown to yield accurate results for ground and electronically excited states of molecules including atoms across the whole periodic table and for arbitrary molecular structures.[87–94]

CASSCF is in principle a Multiconfiguration Self-Consistent Field (MCSCF) method, which means that it simultaneously optimizes both orbitals and CI coefficients for a wave function composed of many configurations. All possible configurations are included which can be formed by distributing a specified number of active electrons among a subset of occupied orbitals, the active orbitals, in a way consistent with spin and symmetry of the state. To the user, this presents a calculation that can be specified similarly as a closed-shell Hartree-Fock or DFT, in terms of basis set and number of electrons. It differs, because also the number of orbitals with full and with fractional occupation, called inactive and active orbitals, respectively, must be specified, together with the spin and point group irrep (symmetry type) of the state(s) to compute. It can, and often does, compute wave functions and energies for many states simultaneously. The orbitals are then optimized to give the lowest possible average energy of these states, whereas the CI expansion coefficients are optimized to describe the individual states.

Although such calculations are in principle possible for arbitrary states and molecules, there remain practical limitations. The most frustrating is the limited size of the active space—the number of orbitals that must be allowed the freedom of variable occupation. It is possible to correlate a few electrons in a large number of orbitals (like in a Multireference CI calculation, say), but usually the number of correlated (active) electrons is comparable with the number of active orbitals, and there is then a drastic increase in the size of the CI expansion with the number of active orbitals. One may have to reduce ones ambitions and compromize, and a calculation that is barely possible can still be missing active orbitals of importance. Unfortunately, compromizing by omitting even one or two orbitals from the preferred active space often results in optimization problems of similar kind as for the early selected MCSCF calculations.

The RASSCF/RASPT2 Concept

When CASSCF/CASPT2 is impractical due to a large number of configurations, restrictions on the CI expansion space can be applied. In the RASSCF (Restricted, instead of Complete) method,[21,22] the number of active orbitals, can be much increased by subdividing the active space into three parts, denoted RAS1, RAS2, and RAS3. The CI space is most easily described as arising from a smaller primary set of configurations by allowing also some excitations from this space. In the primary space, the RAS1 orbitals are fully occupied, the RAS3 orbitals are unoccupied, and the RAS2 orbitals play the role of active orbitals for the primary configurations, which should be those that are essential for describing the nondynamic correlation. The full set of configurations are then those that differ from the primary set by allowing at most a specified number of electrons to be excited out of the RAS1 space, and at most a specified number of electrons excited into the RAS3 space. The full set of configurations thus described is used in the calculation; there is no difference in treatment of primary and excited configurations, and this subdivision is done just to describe the structure of the CI space.

This method was implemented from the start in the currently used program, but it has been used mostly for CASSCF calculations, which are thus regarded as a special case of RASSCF. The reason is partly that true RASSCF calculations usually require some

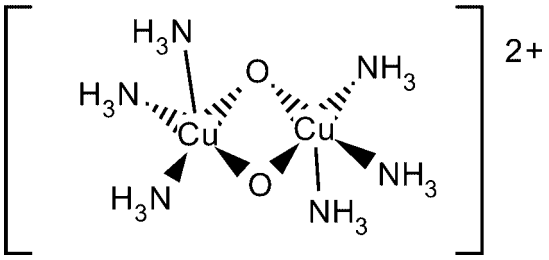

Figure 7. The copper-bis(μ)oxo complex.

experimentation and "hands-on" preparation of starting orbitals to converge to an acceptable solution, and that convergence can be slow and capricious. The extension of the CASPT2 concept to compute perturbative dynamic correlation also from an unperturbed wave function of the RASSCF type is naturally called RASPT2. A first implementation was made by Celani and Werner[95] in a multireference configuration interaction, (MRCI) program.

In contrast to CASPT2, there is yet little experience of the more general RASPT2, but it has now been implemented as a modification of the CASPT2 program used in MOLCAS, and was found useful, e.g., in the study of some copper complexes of biological interest. It has been found that, in order to properly describe the relative energetics, a second d-shell with correlating orbitals is necessary. This requires ten active orbitals per transition metal atom, in addition to any further active orbitals needed for excited states and/or bond breaking. The copper-bis(μ)oxo complex in Figure 7 could not be well described with less then 32 active orbitals with 28 electrons. A CASSCF wave function would have comprised on the order of 10^{17} determinant functions, but the calculation could be done to satisfaction using RASSCF/RASPT2.[96]

Apart from the obvious advantage of allowing a larger number of active, i.e., nondynamically correlated orbitals, there are complications that the user should be aware of. While the CASSCF/CASPT2 method is now a standard tool for many types of calculations, it is not a "black box" method. This is even more true for the RASSCF/RASPT2 combination, and a user may need some background of technical details.

RASPT2: Technical Issues

At present, a CASPT2 or RASPT2 calculation can be roughly divided up into three phases: computing a zeroth-order Hamiltonian for the perturbation expansion; solving the equation system that gives the amplitudes describing the perturbation; and finally using these to compute energies and other properties of interest.

In principle, CASPT2 and Multi-State CASPT2 solves a set of equations of the usual Rayleigh-Schrödinger type

$$\left(\hat{H}_0 - E_0\right)\left|\Psi^{(1)}\right\rangle = \left(\hat{H} - E_0\right)\left|\Psi^{(0)}\right\rangle \tag{21}$$

$$\left|\Psi^{(1)}\right\rangle = \sum_{P=1}^{M} c_P \hat{X}_P \left|\Psi^{(0)}\right\rangle \tag{22}$$

where $\hat{H}_0$ is an approximation to $\hat{H}$, which is a second-quantization representation of the true Hamiltonian. $\Psi^{(0)}$ is the unperturbed wave function, which is a RASSCF wave function. $\Psi^{(1)}$ is the first-order wave function, which is parametrized in terms of a set of excitation operators, $\{\hat{X}_P\}$, acting on $\Psi^{(0)}$, and E_0 is the energy expectation value of the RASSCF wave function. The right-hand side is contained in the so-called interacting space, which is spanned by all wave functions generated by the terms of the Hamiltonian when acting on $\Psi^{(0)}$, orthogonal to $\Psi^{(0)}$ itself. Identically the same space is spanned by the terms comprising the expansion of $\Psi^{(1)}$, which means that the equation can be solved exactly provided that the interaction space is a stable space for the action of $\hat{H}_0 - E_0$.

This parametrization is very much smaller than an equivalent expansion in terms of individual Slater determinants, because each term is comprised of a number of contributing determinants generated from Ψ_0. As a typical application, consider a CASSCF calculation with 12 active electrons in $n_A = 12$ active orbitals, singlet, which has $n_I = 40$ inactive orbitals and 400 basis functions, thus $n_V = 348$ virtual orbitals. The wave function consists of about 800,000 determinants; the number of determinants in the interacting space would be on the order of 10^{15} determinants, but the number of parameters M is just slightly larger than for corresponding MP2 or CCSD calculations from a single determinant. Even so, the equation system is much too large for direct solution, unless simplified.

The ideal simplification would be a diagonal equation matrix, like for usual MP2. For a number of reasons, this is not quite possible for a multiconfigurational $\Psi^{(0)}$. First, the $\Psi^{(0)}$ function can then not be the eigenfunction of a one-electron Hamiltonian, which is required by the perturbation equations. This is, however, rather simple to fix, by taking $\hat{H}_0$ to be a Fock-type Hamiltonian, but removing by projection any coupling between $\Psi^{(0)}$ and its complement. Second, the $\hat{H}_0$ should be a continuous function of $\Psi^{(0)}$, but not of its representation in terms of orbitals, as these can vary more or less arbitrarily while still (by varying the CI expansion) representing the same wave function. The program must then be prepared for the fact that such a Fock matrix is not necessarily diagonal in the RASSCF orbital basis. This is not a very difficult problem, and the CASPT2 program solves it by recomputing internally the CI expansion to correspond to the internally used orbitals, and these can be chosen such as to diagonalize the inactive/inactive, the active/active, and the virtual/virtual subblocks of the Fock matrix, thus defining at least quasi-canonical orbitals and orbital energies.

The remaining nonzero Fock matrix elements are usually quite small. Assume for a while that they are. Then, a third problem is that even with a diagonal one-electron Hamiltonian, the representation of the $\hat{H}_0 - E_0$ operator is far from diagonal. However, it turns out that if the remaining nonzero coupling elements of the Fock matrix can be neglected, the equation system can be factorized into diagonal parts, at the price of an initial full diagonalization of a few matrices. The equation system can be blocked up into subsets, classified by the number of electrons excited from the inactive space, and the number excited into the virtual space, by the excitation operators. The blocks are of varying size. As an example, there is on the order of $n_A^3 n_V$ excitation operators which transfer an electron from the active to the virtual space, as a double excitation of this nature also must excite an electron within the active space. By diagonalizing a matrix of size $n_A^3 \times n_A^3$, these equations can be factorized into an active and an inactive part, yielding MP2-like equations, which can be immediately solved.

In the above example, it turns out that two large matrix diagonalizations dominate. In order to generate the 1728×1728 matrices, we must compute up to three-body density matrices (with active indices only), and then diagonalize two such matrices: the time taken is a matter of seconds, if a good linear algebra library is used. However, the work scales as the number of determinants times n_A^3 for the density matrices, and then n_A^9 for the matrix diagonalization. Doubling the active space will take 500 times as long time for this step, even if the number of determinants is kept reasonable by applying RAS restrictions. Even this size is acceptable, but going further is costly.

Returning now to the remaining nonzero coupling elements of the Fock matrix, these introduce coupling of the equations. However, the equation system can still be solved, by using a Preconditioned Gradient (PCG) solver. This turns out to solve the equation system, in most cases in about 8 to 10 iterations.

Thus, the RASSCF/RASPT2 method is able to form the required matrices, as long as the number of determinants can be kept reasonable (a few million determinants, say), and diagonalize them, as long as the n_A^9 time does not become prohibitively large.

There is one important caveat related to the use of average-state optimized RASSCF wave functions. For the RASPT2, similar restrictions as for CASPT2 apply in the diagonalization of the one-electron Hamiltonian (essentially a Fock-type matrix, giving orbital energies if diagonalized), but now they also invalidate orbital rotations between the different RAS subspaces. The remaining coupling terms between matrix blocks are taken care of, in the CASPT2 case, by the PCG iterations. In the RASPT2 case, the coupling between RAS subspaces is not handled this way, but these elements are ignored. They are generally quite small, for single-state optimized wave functions, but may become large for average-state calculations. This is easily seen in smaller experiments, where the allowed number of RAS1 holes and RAS3 electrons can be increased until the calculation becomes formally identical to a full CASPT2 calculation, yet the results differ. This difference is caused by the inability, in the RAS case, to remove subspace coupling within the active space.

As the correlation completely *within* the active space (such as a double excitation from the RAS1 to the RAS3 orbitals) is assumed to be sufficiently handled at the RASSCF level, additional such excitations are not included in the RASPT2. For a CASSCF wave function, such excitations would be outside of the interacting space, as the unperturbed state has already been obtained as an eigenstate of the CI. But in the RASSCF case, such excitations will be necessary if the restrictions are too restrictive. Also this problem will in general become more severe with average-state calculations. Including such excitations in the RASPT2 is not infeasible, but technically complicated. Also, within the current formulation of the $\hat{H}_0$, this would necessitate computing four-body density matrix elements, which is very costly for large active spaces.

RASPT2 Summary

In conclusion, the RASSCF/RASPT2 method is obviously useful in the cases where the size of the active space is otherwise preventing a regular CASSCF/CASPT2 calculation. However, there is still a lack of experience with regard to the proper way of doing these calculations. What has been already observed is that the number of RAS1 holes and RAS3 electrons should be even, and RAS2 orbitals and electrons are used for qualitatively correct description of any multiconfigurational character and/or configuration differences among states. This also makes sense if the RAS1 and RAS3 spaces are regarded to compute correlation of a mixed dynamic/nondynamic character, or dynamic correlation that is strongly coupled to the nondynamic correlation. So far, the approach has usually been to allow two holes in RAS1 and two electrons in RAS3, which is usually denoted as "SD", and if affordable, four of each (SDTQ). However, for good reasons, the orbital optimization in the RASSCF becomes problematic in the latter case. We would recommend that SDTQ calculations are performed using RASSCF orbitals from the SD calculation, without further reoptimization. Also, what about calculations with, e.g., up to four holes, but allowing only two electrons? Also, is the "even-number" restriction *always* the best? The field is open for experiments.

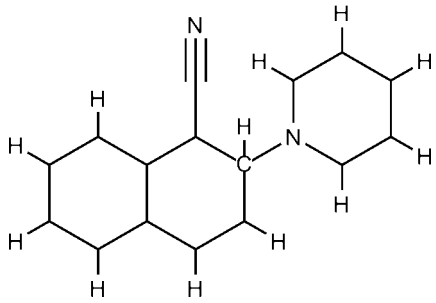

Figure 8. 1-cyanonaphtalene/pyridine exciplex.

For a final illustration, consider a recent study [Roos, private communication] of the exciplex shown in Figure 8. This is a stable molecule as long as it remains in an electronically excited state, but once deexcited it falls apart. The potential energy curves of the three lowest states are shown in Figure 9, and are very similar using CASPT2 and RASPT2. The CASPT2 result was obtained with great effort, almost at the limit of what can be done. The RASSCF/RASPT2 is fairly fast and well behaved. The relevant part of the potential curves is the region around equilibrium of the upper (excited) states, and the dissociative lower (ground state) curve. These parts are virtually the same for CASPT2 as for RASPT2, whereas some small discrepancies can be seen for the excited states at the longer CN distances.

Coupled Cluster Techniques in MOLCAS

The Coupled Cluster (CC) theory is one of the most powerful tools for obtaining accurate molecular energies and molecular properties with a high and controlled accuracy. As Čížek's formulation of this theory for many–electron systems in 1966, we have witnessed impressive development of this approach.[97–102] The key point behind the success of the CC method lies in expressing the wave function in an exponential form, $|\Psi\rangle = e^T|\Phi_0\rangle$, where T is a many–electron excitation operator and $|\Phi_0\rangle$ is a reference wave function. Most routine CC calculations exploit the single–determinant Hartree–Fock wave function as a reference. The progress in the CC formalism with a many–determinant reference

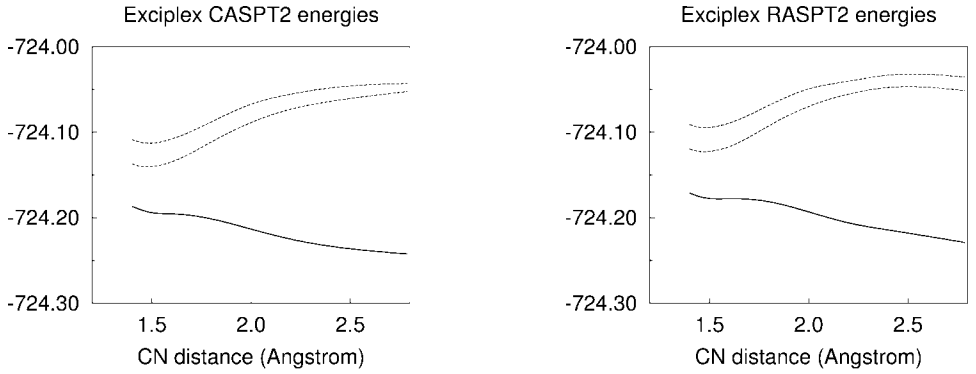

Figure 9. The potential energy with varying C–N distance, for CASPT2 and RASPT2.

or more general Multi-Reference (MR) wave function, reasonable methods for the treatment of quasi-degenerate systems, is impressive[98,102–107] but MR CC methods still remain demanding for large–scale applications. Therefore, we feel that for treating quasi-degenerate systems, general potential energy surface and dissociation processes, CASPT2, RASPT2, MR-CI, and similar methods, available in MOLCAS, are still preferable. On the other hand, when the system can be well represented by a single determinant reference (or by a defined fixed linear combination of a few determinants), CC methods yield accurate results in a straightforward and computationally efficient way.

The wave function expressed in an exponential form leads to faster convergence of the energy and of the wave function compared with wave functions based on the linear expansion ansatz. Also, the exponential ansatz guarantees that the method is size–extensive. The most widely used single–determinant CC method for accurate molecular calculations is CCSD(T)[108] in which the excitation operator T in CCSD is approximated as $T = T_1 + T_2$. The amplitudes of the single and double excitation operators, t_i^a, t_{ij}^{ab}, are optimized iteratively, and are exploited in the next step for a perturbative treatment of triples.[109] Most demanding steps in CCSD scale as $N_o^2N_v^4$ and $N_o^3N_v^3$. Computational requirements for noniterative triples scale as $N_o^3N_v^4$ and $N_o^4N_v^3$, fortunately in a single (noniterative) step. N_o is the number of occupied orbitals (OO), N_v is the number of virtual orbitals (VO). N is used if there is no need to distinguish between occupied, virtual, or total number of orbitals. The next step in the hierarchy of CC methods is the full iterative account of triples in CCSDT[110] in which T is approximated as $T = T_1 + T_2 + T_3$. The method needs summations over eight indices in an iterative process and storing triples amplitudes. To alleviate computational demands of the full iterative CCSDT, various approximations of the disconnected clusters in the exponential expansion of $e^{T_1+T_2+T_3}$ were introduced[109,111] leading to methods like CCSDT-1, CCSDT-2, CCSDT-3. Approximations keep the hierarchy of the orders of the CC wave function.[100]

For the Coupled Cluster correlation energy, E_{CC}, we need only the single and double excitation operators amplitudes, t_i^a and t_{ij}^{ab}. The energy formula is the same irrespective of the approximation of T beyond $T = T_1 + T_2$:

$$E_{\mathrm{CC}} = \left\langle \Phi_0 \middle| \left[H_N e^{(T_1+T_2)} \middle| \Phi_0 \right\rangle \right]_C = \left\langle \Phi_0 \middle| \left[H_N \left(T_1 + T_2 + 1/2 T_1^2 \right) \middle| \Phi_0 \right\rangle \right]_C \quad (23)$$

H_N is the Hamiltonian in the second quantization form, the index C means that only connected diagrams are considered in the diagrammatic representation of eq. 23.[97–101] Much more demanding is calculation of the excitation amplitudes needed in eq. 23. Equations for α-excited amplitudes are obtained by projecting the wave function onto the respective $\langle \Phi_\alpha |$ excited state determinant, i.e.,

$$\langle \Phi_\alpha | [H_N e^T | \Phi_0 \rangle]_C = 0. \quad (24)$$

Also here is the exponential expansion restricted due to the fact, that H_N contains merely one– and two–electron terms. When projecting onto the double excitation equations in CCSD amplitude equations, no higher than products of T_n operators representing quadruple excitations are needed. Similarly restricted are equations defining higher excitations amplitudes. In spite of this restriction, in CCSDT and higher level CC methods the number of terms increases tremendously and the story starts to be very complicated. Algebraic representation can be obtained by using diagrammatic techniques and the second quantization formalism, leading to the string-based coupled cluster theory and automated generation of computer codes, as pioneered by Li and Paldus[98,112] and fully exploited by Kallay and Surjan.[113] Another advantage of the diagrammatic representation of CC equations is its transparency. It is particularly useful for the wave function analysis[98–101] when considering approximations within a particular selection of the excitation operator T. What we would like to stress here is the fact that the CC theory allows a hierarchy of the order–by–order approximations to the wave function and the energy in terms of the perturbation theory, which is a key for a controlled accuracy.

Clearly, CC methods, as most other wave–function (WF) quantum chemistry methods, cannot compete in efficiency with DFT methods. Presently, DFT methods dominate the computational chemistry calculations of large molecules because their scaling with the number of electrons is more favorable. Yet the importance of the wave function methods as a tool for obtaining accurate results with controlled accuracy can be hardly overestimated. Moreover, reliable CC or other WF data serve as benchmarks for DFT methods for which controlled accuracy is more difficult. Progress in DFT brings plenty of different functionals, often developed to describe specific problems or particular molecular properties. Obviously, it is preferable if CC reference data are available for larger molecules which are closer to species calculated by less demanding DFT

calculations. To serve this purpose better, we need CC methods, particularly CCSD(T) with enhanced efficiency within MOLCAS.

Open–Shell Calculations

The open–shell CC program in MOLCAS was primarily developed for efficient treatment of the high–spin systems which can be well represented by a single–determinant Restricted Open–shell Hartree–Fock (ROHF) reference. The two determinant CCSD method is introduced in MOLCAS for treating excited singlets.[114] As the contribution from triples is still missing, this part of the code is not widely used so far. Starting point of our high–spin implementation is the spin–orbital formulation of Stanton et al.[115] Fully relying on the spin-orbital formulation means, first, lower efficiency, as one has to manage spin–orbitals instead of orbitals and, second, resulting CCSD(T) energy is affected by the spin contamination even if we use the ROHF reference orbitals. We also note that the ROHF reference function is not uniquely defined. There is certain degree of freedom in construction of the one–electron part of the Hamiltonian, f_R, which does not change the SCF energy, but affects orbital energies. The iterative CCSD procedure itself is fully invariant to splitting of the Fock operator $f = f_R + u$. However, perturbative energy terms are not, due to using orbital energies in denominators. Therefore, also noniterative T3 contribution, evaluated in a perturbational manner, slightly depends on the selection of the reference function and the denominator. For details, see e.g. ref. 116,117 and careful discussion in ref. 118

The ROHF reference function is an eigenfunction of the spin operators S^2 and S_z, but the CC wave function $exp(T)|\Phi_0\rangle$ is not, if the CC expansion (or the T operator) is not complete. The magnitude of the spin contamination diminishes with higher levels of the excitation operators. Amplitudes of the single and double excitation operators in CCSD, t_i^a, t_{ij}^{ab}, must be spin adapted. Spin adaptation (SA) also reduces the number of independent parameters (i.e., excitation amplitudes), by about a factor of three for CCSD, and enhances the efficiency, if fully exploited. In our implementation in MOLCAS we have profited from the work by Takahashi and Paldus.[119] We employ an approximate SA, particularly the simplest form in which only T_2 amplitudes, labelled by inactive and secondary orbitals are adopted (active orbitals would be singly occupied MOs, using the terminology of CASSCF). This approximate method[116,117] preserves most of the advantages of the spin adaptation, is sufficiently accurate (compare with exact results by Gauss and Szalay[120]) and the formulation is the same for any multiplet. Effects of the spin–adaptation in molecular properties are usually small. More difficult cases, like CCSD(T) calculation of the electron affinity of the CN or O_2 molecules require SA for accurate results.

Efficiency of CC Calculations

The present version of the MOLCAS package contains two implementations of CCSD(T) method: An older code, described already in previous MOLCAS paper[26] and a new one, based on Cholesky decomposition of the two–electron integrals. The old implementation of the CCSD method was based on the formulation[115] which exploits spin–orbital formalism aimed toward minimizing the overall number of floating-point operations. The code exploits orbital spatial symmetry and is compatible with both RHF and ROHF reference functions. It is optimal though for open–shell molecules only, whereas a different algorithm could exploit simplifications arising in the closed–shell case. Program handles arrays up to the size of $N_o^2 N_v^2$ in an unsegmented form, which ensures relatively small computational overhead. This feature, combined with the efficient matrix–matrix oriented formulation and BLAS (level 3) routines guarantees high performance of the arithmetical part. Being completely MO based, this algorithm required storing all MO integrals (proportional to N^4) on disk. Also memory consumption cannot be arbitrarily reduced, as the $N_o^2 N_v^2$ arrays are treated as unsegmented. Moreover, the way the code was parallelized, allowed efficient (close to linear) scaling only up to 8–16 nodes. All these factors cause serious limitations of its applicability. Typically, calculations do not exceed 500 virtual orbitals and the performance strongly depends on the computer hardware, the number of the correlated electrons, computational symmetry, and the distribution of molecular orbitals within irreducible representations of the symmetry point group. To further enhance the applicability of the CCSD(T) method, a completely new code was implemented. It is based on two novel ideas, mainly the Cholesky decomposition of two electron integrals and the segmentation (or blocking) of the virtual orbital space (VOS).

To reduce or, eventually, completely eliminate the memory limitations and to utilize efficient parallelization we decided to split the VOS into N' segments, each having $N_{v'} = N_v/N'$ orbitals. Memory requirements are dramatically reduced, since for all intermediates having at least one virtual index, we can work with their fragments with reduced dimension of $N_{v'}$ instead of N_v. This affects mostly the time consuming N^6 matrix multiplications, which are split into N'^2 "independent" subjobs of almost the same size. As a byproduct, splitting offers a possibility for the efficient (almost linear) parallelization, employing up to N'^2 computational nodes. However, parallelization and segmentation of the VOS brings in some additional overhead, due to repeated (mostly I/O) operations connected with the segmentation in the matrix multiplication process. The only internode transfer required in this new CCSD algorithm is the transfer of T_1 and T_2 amplitudes in each iteration. The wall–clock time needed for this transfer increases with the number of parallel nodes, though less than linearly. Thus, due to this connection of segmentation and the number of parallel tasks, proper N' needs to be selected (presently as a user-defined parameter) to meet the memory requirements and to ensure efficient parallelization.

Cholesky decomposition of integrals cannot, in general, reduce the scaling of the most time consuming steps in the CC methods. However, storing only the (MO-transformed) Cholesky vectors alleviates one important bottleneck of the CCSD(T) approach, e.g., the storage of the 2-electron integrals, and offers additional flexibility whenever the reconstruction of these integrals is needed. This concerns mainly the $(VV|VV)$ (scaling as N_v^4) and $(OV|VV)$ (scaling as $N_v^3 N_o$) integral types, where V stands for arbitrary index of virtual orbital and O for the occupied one. A different treatment to avoid the disk bottleneck, widely used in other CCSD codes, is so called "integral direct" algorithm,[121] which essentially calculates on–the–fly all the required AO integrals. These approaches have, however, a disadvantage compared with our MO Cholesky vectors based CCSD code that, the CCSD equations are solved in the AO basis and cannot profit so much from the truncation of the virtual orbital space either via OVOS method of Frozen Natural Orbitals, see further.

In our new CCSD code, two basic algorithms for treating the most demanding $(VV|VV)$ integrals are implemented and are available on user's choice. Both employ segmentation governed by the size of the $(V'V'|V'V')$ block. In the first approach we do not store any integral files larger than $N_o^2 N_v^2$ on the disk and desired integral blocks are recalculated from Cholesky vectors, eq. 12, on the fly. This yields enormous savings of the disk space, but overall arithmetical demands increase. On the other hand, this "purely CD based" approach, with suppressed I/O and extended arithmetics can better exploit modern multi-core architecture of the nodes, than the "integral based" one. In the alternative "integral based" approach we precalculate most of the MO integrals (including $(VV|VV)$) from the Cholesky vectors, eq. 12, before the CCSD iterative procedure and store them on the disk. Taking advantage of how the Cholesky decomposition of the two-electron integrals is implemented in the parallel version of MOLCAS, namely that Cholesky vectors are generated on each computational node in blocks according to the segmented auxiliary index, precalculation of above mentioned integrals can be efficiently parallelized as well. CCSD equations are then solved essentially in the "traditional," MO–based way. This "integral based" algorithm is preferable either if there is an abundance of the disk space, or in the massively parallel runs, where due to the way the algorithm is implemented, only a small portion of the MO integrals needs to be stored on each parallel node. For smaller calculations it is typically faster than "purely CD based" approach, however, for truly large scale calculations with N_o^2 comparable to M (dimension of the Cholesky auxiliary index), "purely CD based" approach becomes preferable. MO transformed Cholesky vectors are also employed in the elimination of tedious manipulations with the $(OV|VV)$ integrals. Several terms, containing this type of integrals, can be treated together with terms containing $(VV|VV)$ integrals in a single step. The rest of these terms can be reformulated using L_{pq}^J vectors. Even if the scaling is not reduced, any manipulations with $(OV|VV)$ integrals can be fully avoided in this way. For example, the contribution

$$t_{ij}^{ab} \leftarrow \sum_c (ai|bc) t_j^c \tag{25}$$

can be performed as

$$A_{bj}^J = \sum_c L_{bc}^J t_j^c \tag{26}$$

$$t_{ij}^{ab} \leftarrow \sum_J L_{ai}^J A_{bj}^J \tag{27}$$

Procedure 26–27 needs $MN_oN_v^2 + MN_v^2N_o^2$ operations, i.e., about M/N_v times more than procedure 25, however manipulations with $(OV|VV)$ integrals is completely eliminated. The excess of the arithmetics is not large, because all terms of this kind scale at most as N^5.

Generally, efficiency of parallelization of the CCSD algorithm depends on the size of the system. It is efficient, if the "wall–clock portion" of calculation of the N^6 steps on each node is larger than the overhead resulting mostly from the internode data transfer, which scales basically as N^4. The larger the system is, the more efficient is the parallelization, as the calculation spends less time with the data transfer. For a systems with about 1000 basis functions, our new CCSD code is efficient even for hundreds of parallel nodes. Performance of the new code will be described in details elsewhere (Neogrády et al., to be published).

For systems with large number of correlated electrons, the noniterative (T) part becomes by far the most time consuming step. For evaluation of the (T) contribution, our new CCSD code was extended with the essential routines adapted to MOLCAS from the code programmed by Noga and Valiron.[122] Also here, segmentation of the VOS is used. Algorithm for (T) can be very well parallelized, because it can be split into large number of independent subjobs, with almost no communication among the nodes. Number of subjobs depends on the number of occupied orbitals, not on N'. Much more efficient parallelization can be achieved, compared to the CCSD step, which can to some extent compensate its order–of–magnitude higher scaling (N^7), almost prohibitive for large calculations.

The new suite of CC codes is presently fully implemented only for closed shell systems in the spin integrated form[123] with the minimized number of arithmetic operations. A code, with a similar capabilities, for open–shell systems is currently under development. Several groups tried to resolve limitations of conventional CCSD(T) approaches. Gordon,[124] Pulay[125,126] and Bartlett[127] and their coworkers have announced new implementations of the CCSD(T) codes optimal for massive parallelization and memory requirements. Comparison of the efficiency of various implementations is not available to us. Concerning new approaches for perturbative triples, several appealing attempts were published during the past few years. A common feature of these approaches is the decomposition (either in the Laplace or Cholesky fashion) of the energy denominators. Although the Cholesky decomposition–based approach by Koch et al.[128] seems to be more efficient for systems with high ratio of occupied to virtual orbitals, Laplace decomposition–based approaches suggested by Scuseria and Head-Gordon groups utilize prescreening of certain intermediates transformed to either Natural Orbitals[123,129] or into localized, atom-labelled projected orbital basis[130]). Both approaches have capability of reducing the scaling of perturbative triples from N^7 to N^5, but more robust implementations are desirable for extensive applications.

Optimizing and Reducing the Space of Virtual Orbitals (OVOS)

Cholesky decomposition and high level of parallelism is a prerequisite for using CCSD(T) within MOLCAS for larger applications than it was possible before. Nevertheless, we still need to look at alternative ways leading to reduced computational demands. Unfavorable scaling with the number of virtual orbitals N_v^4 in most difficult steps in CCSD and triples makes calculations with large N_v quickly prohibitive. Another bottleneck is the number of occupied orbitals when we need to correlate large number of electrons. Large N_v frequently occurs in calculations with extended (diffuse) basis sets for accurate calculations of, say, response properties, excited (particularly Rydberg) states, electron affinities, dispersion interactions, etc. Do we really need an extended full space of virtual orbitals selected with no condition other than being orthogonal to (canonical) HF occupied orbitals? The simplest way, deleting just a few virtuals with highest orbital energies is of little help. Truncation of VOS to a significant fraction, say one half, may already reduce the N_v^4 steps by a factor

of 16. This can be achieved by a suitable rotation of virtuals. We can construct such a transformation of virtual orbitals that "maps" the effect of the full space of virtuals into a smaller subspace without significantly loosing the accuracy. We tested several optimization criteria in previous work[25] based on the idea of using Optimized Virtual Orbital Space (OVOS) proposed long ago by Adamowicz and Bartlett.[131,132] Our newly implemented optimization is based on the maximum overlap of the wave function in the full virtual orbital space (VOS) and the wave function in the truncated OVOS space. The simplest implementation employs the first order wave function, but the same idea can be used for any wave function.[25] For example, the maximum overlap based on the CCSD wave function can in principle be used for optimization of OVOS for higher levels of the CC theory, like CCSDT or CCSDTQ. Returning back to the first–order wave function our overlap integral is

$$L = \left\langle \Phi_0 \middle| T_{\mathrm{MP2}}^{\mathrm{FULL}} | T_{\mathrm{MP2}}^{\mathrm{OVOS}} \middle| \Phi_0 \right\rangle \tag{28}$$

To ensure the orthonormality of the transformed set of orbitals, we supplement the functional with the Lagrangian multipliers which leads to a new functional, which is actually optimized. Within OVOS, eq. 28, the $T_{\mathrm{MP2}}^{\mathrm{OVOS}}$ operator is defined as

$$T_{\mathrm{MP2}}^{\mathrm{OVOS}} = 1/4 \sum_{\substack{i,j \\ a^*,b^*}} t_{ij}^{a^*b^*} a^{*\dagger} i b^{*\dagger} j + \sum_{i,a^*} t_i^{a^*} a^{*\dagger} i \tag{29}$$

whereas the corresponding $T_{\mathrm{MP2}}^{\mathrm{FULL}}$ operator is defined in the full virtual space. For closed shell molecules the last term in eq. 29 is not needed. Indices with an asterisk correspond to virtual orbitals of the truncated OVOS space. In our calculations, we usually refer to the dimension of OVOS in terms of percentage compared with the dimension of the full VOS. Target truncation of VOS is 60 or even 50% with respect to the full VOS. Obviously, any specific percentage is just a rough estimate since orbitals must be truncated keeping in mind the equivalent symmetry orbitals and other aspects of the VOS structure. In calculations in which we calculate the energy difference (as, e.g., in interaction energies), we assure a balanced reduction of the virtual space by, e.g., requiring that for any specific truncated OVOS the percentage of the value of the optimization functional, eq. 28, with respect to the full VOS, is the same for all participating species (dimer, monomer, ...). Of great help is the inspection of eigenvalues of the set of equations to which the optimization procedure leads. For details see refs. 25, 133–135. The response CC theory using OVOS was introduced by Boman and Koch.[136] We also note that the OVOS technique is closely related to truncating the virtual space transformed to the Frozen Natural Orbitals (FNO).[137,138] There are several alternative ways of reducing the computer demands in CC calculations. One possibility is based on explicitly correlated CC-R12 theory[139] which allows using smaller basis sets yet leading to very accurate results. Another possibility was proposed by Werner and Coworkers[140–142] and others, based on transformation to the localized orbitals.

CCSD(T) method is since long routinely linked with scalar relativistic DKH calculations as described in Part 4. Large basis sets are typical for relativistic calculations. Since for heavy elements we keep large number of inner shell electrons frozen, OVOS is very useful in these applications. OVOS is useful also in relativistic calculations which need uncontracted basis sets. This occurs when we calculate relativistic effects using a particular Hamiltonian for which a specific contracted basis is missing. One example are effects related to the change of picture, see Part 4. Examples of using OVOS in relativistic calculations are presented in ref. 133.

Table 2. Benzene and Uracil Dimer Stabilization Energies [kcal/mol] for Various Structures Using Dunning's aug-cc-pVXZ Basis Sets.[145]

Benzene dimer[a,b]	PD	TT	T	S
Basis set/(number of used virtual orbitals)				
aug-cc-pVDZ 100%/(342)	2.15	2.44	2.28	1.27
aug-cc-pVTZ 70%/(≈ 550)	2.49	2.66	2.57	1.51
aug-cc-pVQZ 60%/(≈ 836)	2.63	2.75	2.65	1.61
Uracil dimer[c]	H-bonded		Stacked	
Basis set/(number of used virtual orbitals)				
aug-cc-pVDZ 100%/(382)	18.43		8.54	
aug-cc-pVTZ 60%/(≈ 568)	19.81		9.33	

"%" represents the fraction of optimized virtual orbitals active in the correlation energy calculation. No point group symmetry was applied in computation.
[a]PD, parallel displaced, C_{2h}, TT, T-shaped tilted, C_s, T, T-shaped, C_{2v}, S, "Sandwich," D_{6h}. Dimension of OVOS slightly varies with the structure.
[b]Sixty correlated electrons.
[c]Eighty-four correlated electrons.

Benchmark CC Calculations Within MOLCAS

Robustness of the Cholesky-based CCSD(T) code implemented in MOLCAS is demonstrated on calculation of weak noncovalent interactions. This is a very tough task, especially when the energy is controlled by dispersion interactions, for which highly correlated methods with large augmented basis sets are needed. Two examples, the benzene[143] and uracil[144] dimers are presented in Table 2.

We stress the importance of using high level of correlation including triples in CCSD(T). The stabilization energy for, e.g., the PD structure of the benzene dimer at the MP2 level, 4.26/4.68/4.82 kcal/mol with aug-cc-pVTZ/aTZ/aQZ basis sets is strongly overestimated. It is underestimated with CCSD, interaction energies being 0.96/1.17/1.28 kcal/mol for the same structure and the basis sets. Analogous conclusions can be made for the stacked structure of the uracil dimer, with MP2 and CCSD stabilization energies 9.80/10.63 and 6.83/7.52, respectively, with aug-cc-pVDZ/aTZ basis sets.

Extended basis sets CCSD(T) calculations of the benzene and uracil dimers were tractable with standard computer resources thanks to employing the OVOS technique. Calculations of the uracil dimer with OVOS truncated to 60% with the aug-cc-pVTZ basis set were demanding (21 iterations of the CCSD part took 40 wall-clock hours on 5 quad core 2.4 GHz computational nodes), but truly difficult was the triples part taking 168 h with the same setup. Considering that triples scale as N_v^4 using of the OVOS method leads to speedup by almost an order of magnitude (80%), saving more than 1000 h. Calculations of similar systems with, say, 80 correlated electrons and using up to 1500 contracted Gaussians are presently feasible but the computer time is certainly not short. Cholesky decomposition and high level of parallelism is inevitable in large–scale CC calculations.

Table 3. Spin–Adapted ROHF CCSD(T) Adiabatic Electron Affinities of the Oxygen and Uracil Molecules [eV].

Electron affinity of the oxygen molecule, $^3\Sigma_g^-$				
Basis set/(# of v. o.)	100%[a]	70%	60%	50%
d-aug-ccpV5Z	0.403	0.408	0.410	0.411
d-aug-ccpV6Z	0.407	0.408	0.412	0.418
CBS limit[c]	0.415	0.420	0.421	0.424

Electron affinity of the uracil molecule			
Basis set/(# of v. o.)	100%[a]	70%	60%
aug-ccpVDZ[b]	−0.189(−0.160)		−0.200(−0.177)
aug-ccpVTZ	−0.150	−0.155	−0.157

Dunning's (d)–aug-cc-pVXZ basis sets. "%" represents the fraction of optimized virtual orbitals active in the correlation energy calculation.
[a]One hundred % means full virtual space.
[b]Number in parentheses is with spin–adaptation omitted in CCSD(T).
[c]With vibrational, core correlation, and relativistic corrections is EA 0.449 eV.[146]

Before using OVOS truncated to, say, 60 or 50% of the full virtual space in routine calculations the accuracy should be carefully verified. We calculated[134] interaction energies of several H-bonded and stacking systems, which are models for interactions in biologically relevant molecules. Good performance of OVOS for the hydrogen bonded formamide dimer, particularly with larger basis sets, is demonstrated in Figure 10. OVOS, even when truncated to 50%, reproduces the basis set dependence excellently with 10 times shorter computer time than is needed for the full VOS calculation. Interaction energies with OVOS truncated to 60% are with largest basis sets accurate to within 0.02 kcal/mol.[134] CCSD(T) calculation of the formamide dimer using the aug-cc-pV5Z basis set (1242 contracted Gaussians and 36 electrons correlated) is tractable with so truncated OVOS even with a standard workstation.

High–spin open–shell ROHF–CCSD(T) results are represented by electron affinities (EA) of the oxygen (the $^3\Sigma_g^-$ state)[135,146] and uracil molecules. Data in Table 3 represent the electronic contribution to adiabatic electron detachment (AED) energies. Our full virtual space AED energy[146] of O_2 at 0 K, 0.449 ± 0.008 eV, employing spin–adapted ROHF CCSD(T) calculations with extrapolation to the Complete Basis Set (CBS) limit including zero–point vibrational, core correlation, scalar and spin-orbit relativistic corrections is in superb agreement with recent photoelectron spectroscopy electron affinity measured by Ervin et al.,[147] 0.448 ± 0.006 eV. Extensive CASPT2 and MR CI methods[148] lead to a reasonable EA, 0.389 eV, which deviates from the experimental value by 0.06 eV. CCSD(T) result for AED of O_2 with OVOS truncated down to 50% of the full space reproduces the full space affinity with the accuracy of 0.01 eV.[135]

Calculation of EA for the uracil molecule is a very difficult task both experimentally and theoretically.[149–151] Bachorz et al.[149] report the final value, +40 meV, which includes vibrational and other corrections (+0.155 eV). Our treatment of the effect of the spin–adaptation in CCSD(T) reduces EA of uracil by about 30 meV. This reduces EA to just 10 meV. Basis set effects may enhance this value. Calculations using the aug-cc-pVQZ basis set for the uracil anion are in progress, but due to its puckered structure and thus no symmetry, this task is very difficult. Larger basis sets could be used with MP2 or DFT but both methods are completely unreliable for this problem.[149] Whether the uracil molecule can accommodate an extra electron is, therefore, not yet solved.

The ESPF Method and its Applications in a Hybrid QM/MM Scheme

The MOLCAS package includes various theoretical methods able to include the interactions between a quantum distribution of charges (hereafter denoted as the quantum mechanical (QM) subsystem) and an external electrostatic potential. For instance, point charges, dipoles, and polarizabilities can be explicitly added, hence polarizing self-consistently the QM wave function. When one wants to include isotropic solvent effects, MOLCAS allows to use two different continuum methods (the solvent is modelled as a structureless dielectric continuum): the Kirkwood model based on a spherical solute cavity[152] or the polarizable continuum model (PCM) featuring a molecular shape-dependent cavity.[153] If solid state calculations are concerned, MOLCAS can take into account the periodicity of the system by means of embedding *ab initio* model potentials.[154]

When the molecular system under investigation features some anisotropic short- or long-range interactions (e.g., hydrogen bonds), a microscopic description of the surroundings is required. Fortunately, the locality principle on which all the chemistry relies, allows to exclude from the QM model all the atoms that do not participate directly to the studied electronic process, leading to a partition of the whole system into a QM subsystem and its surroundings. A popular partition scheme, called the Quantum Mechanics/Molecular Mechanics (QM/MM) hybrid method,[155–157] relies on parameterized simple interaction potentials (whose sum is called a force-field) between QM particles and MM atoms. The total energy of the whole system can be decomposed:

$$E = E_{\mathrm{QM}} + E_{\mathrm{MM}} + E_{\mathrm{QM/MM}} \tag{30}$$

where E_{QM} denotes the energy of the QM subsystem, E_{MM} is the energy of the MM subsystem, and $E_{\mathrm{QM/MM}}$ includes all the bonded and nonbonded interactions between both subsystems. Because numerous MM force-fields are already available in various chemistry fields (organic chemistry, biochemistry, heterogeneous catalysis, etc.), the QM/MM method often takes advantage of them. Such a QM/MM scheme has been implemented in MOLCAS and it is briefly presented in the following.

In almost all the current QM/MM implementations, the total electrostatic interaction between the QM and MM subsystems involves classical interactions between the QM nuclei and the MM multipoles (often limited to point charges) and quantum interactions between QM electrons and MM multipoles, thus polarizing the QM wave-function. The one-electron Hamiltonian matrix elements should be modified accordingly:

$$h_{\mu\nu}^{\mathrm{QM/MM}} = h_{\mu\nu} + \langle \mu | V^{\mathrm{MM}}(\mathbf{r}) | \nu \rangle \tag{31}$$

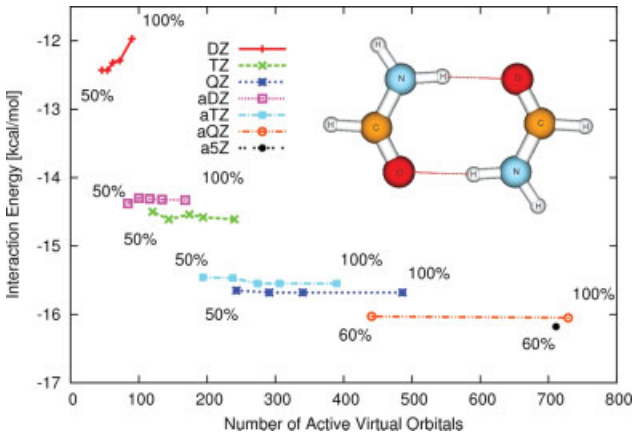

Figure 10. Scaling of the interaction energy of the formamide dimer with number of active optimized virtual orbitals in various (aug-)-cc-pVXZ Dunning's basis sets. Full space of virtual orbitals represents 100%.

for a set of n electrons feeling the external electrostatic potential V^{MM}. When MM point charges q located at positions $\mathbf{r}_q$ are involved, this potential usually takes the form:

$$V^{\mathrm{MM}}(\mathbf{r}) = \sum_q -\frac{q}{|\mathbf{r}-\mathbf{r}_q|} \tag{32}$$

However, this form (eq. 32) presents several disadvantages: the QM/MM electrostatic interaction energy is nonsymmetric by the exchange of the QM and MM subsystems, its computational cost depends on the size of the MM subsystem, it requires that the external potential originates from point multipoles (and often point charges only) and it prevents the use of the standard MM electrostatic tricks, like the use of exclusion rules (the so-called 1–4 conditions) or the use of some switching function leading to inconsistencies in the electrostatic treatment of the QM/MM and MM levels.

To solve these problems, the ElectroStatic Potential Fitted (ESPF) method[158] has been devised and incorporated in MOLCAS. This method is based on the following classical electrostatic interaction energy:

$$E^{\mathrm{elec}}_{\mathrm{QM/MM}} = \sum_{a=1}^{N} Q^a V^{MM}(\mathbf{r}_a) \tag{33}$$

where Q^a are expectation values of distributed multipolar atomic operators $\widehat{Q}^a$:

$$Q^a = Z_a - \langle \widehat{Q}^a \rangle = Z_a - \sum_{\mu\nu} P_{\mu\nu} Q^a_{\mu\nu} \tag{34}$$

with $P_{\mu\nu}$ a density matrix element.

In close analogy with electrostatic potential derived charges (or other higher order multipoles), the matrix elements $Q^a_{\mu\nu}$ of such operators are fitted to the electrostatic potential integrals $V^k_{\mu\nu}$ computed on a grid of points k surrounding the QM subsystem:

$$Q^a_{\mu\nu} = \sum_{ab}\sum_k (\mathbf{T}^\dagger\mathbf{T})^{-1}_{ab} T^\dagger_{bk} V^k_{\mu\nu} \tag{35}$$

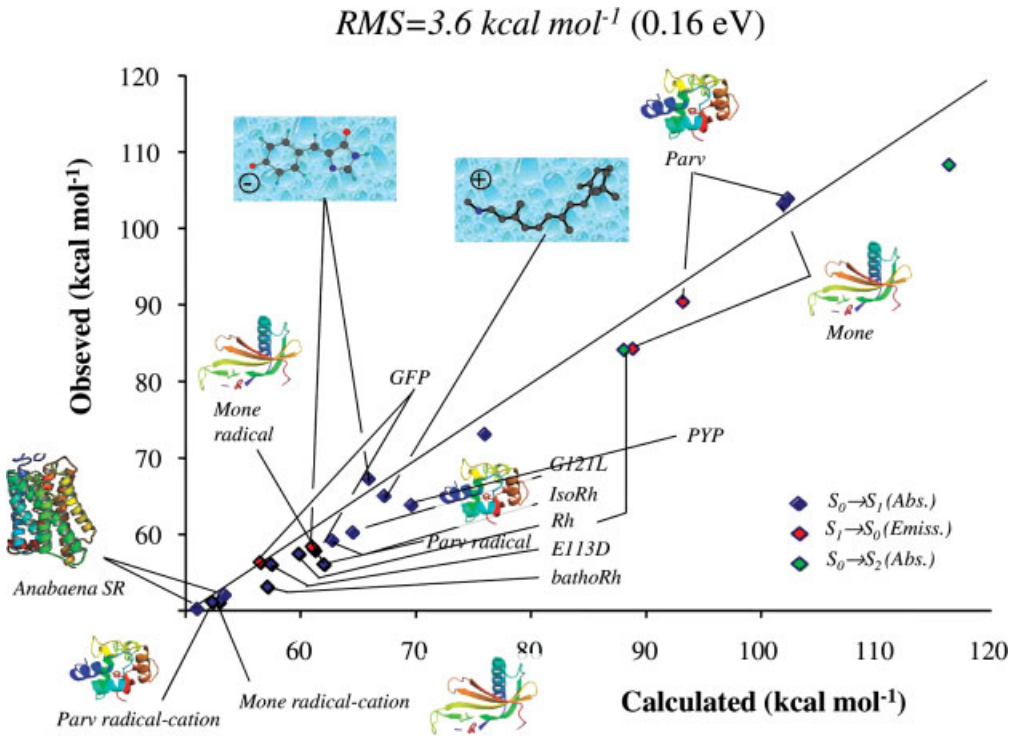

Figure 11. Computed vs. experimental absorption and emission energies of different chromophores in various proteins or solvents.

Table 4. Direct vs. ESPF Deviations in Mulliken and ESPF Atomic Charges (in *e*) and Molecular Dipole Moment (in *D*) of the QM Water Molecule Surrounded by 3999 MM Water Molecules.

	Mulliken charge			ESPF charge			Dipole
	O	H	H	O	H	H	moment
Max. dev.	0.0054	0.0043	0.0047	0.0035	0.0027	0.0033	0.0097
RMS dev.	0.0024	0.0015	0.0016	0.0012	0.0011	0.0011	0.0034

where $\mathbf{T}$ is the kernel matrix for electrostatic interactions, i.e., $T_{kb} = |\mathbf{r}_b - \mathbf{r}_k|^{-1}$ and derivatives with respect to the nuclear coordinates. Hence, in the ESPF method, the one-electron Hamiltonian is different from (eq. 31):

$$h_{\mu\nu}^{\mathrm{QM/MM}} = h_{\mu\nu} + \sum_{a=1}^{N} Q_{\mu\nu}^{a} V^{MM}(\mathbf{r}_a) \tag{36}$$

Hence the ESPF operators are particularly suitable to take into account any type of external electrostatic potential (field and field derivatives), as long it can be computed on each QM atom. Moreover the modification of the one-electron Hamiltonian is now independent of the size of the MM subsystem. This method can be incorporated easily into any QM method already present in MOLCAS. Note also that the first derivatives with respect to the QM atom positions are straightforward, however second derivatives have not been considered yet. The expectation values of the ESPF operators are QM atomic multipoles, i.e., electrostatic potential-derived charges and higher order multipoles. Note the ESPF method can be used to compute such multipoles, even when the external potential V^{MM} is not present.

As a final remark, the ESPF method is an approximate method, as it relies on the order of the multipolar atomic operators $\widehat{Q}^a$. However, tests have shown that even at the lowest order, the agreement between the results obtained using the one-electron Hamiltonian (eq. 31) or the ESPF one (eq. 36) is really good. To demonstrate the accuracy of the ESPF method, the Mulliken charges, the ESPF charges and the dipole moment of a single water molecule (QM level: RHF/STO-3G) embedded in a box containing other 3999 water molecules (MM level: TIP3P model) have been computed using either the ESPF method or by the direct inclusion of the surrounding point charges (using the `XField` keyword). The deviations are then calculated using 112 configurations extracted from a 112 ps molecular dynamics trajectory. The maximum and averaged deviations are reported in Table 4 and perfectly demonstrate the ESPF accuracy.

The ESPF method is the core of the QM/MM scheme implemented in MOLCAS. Non-electrostatic QM/MM interactions have been added by coupling MOLCAS with a modified version of the MM package TINKER.[159†] This MOLCAS/TINKER coupling features the MM microiterations technique that can be used to minimize the MM geometry each QM geometry optimization step. Moreover, the approximate Hessian matrix can include some extra MM degrees of freedom, corresponding to MM atoms located in a sphere defined around the QM subsystem, giving a better convergence in a geometry optimization of the whole QM/MM system. If the QM/MM frontier is located on a chemical bond, the link atom scheme is available to saturate the QM free valence. The link atom position can be constrained using standard geometry constraint available in MOLCAS or using the Morokuma's scheme[160] that features a proportionality constant between the QM–MM bond length and the QM–link atom bond length.

The present QM/MM implementation is currently used by different theoretical chemistry groups, with particular interest toward photochemical studies in biological systems, e.g., in refs. 161–164. An overview of results obtained by Olivucci and coworkers is shown in Figure 11.

Photochemistry and Constrained Optimizations

One of the most significant strengths of MOLCAS is the efficient implementation of multi-configurational methods such as CASSCF, CASPT2, MS-CASPT2, and RASPT2. These procedures are generally applicable to all types of electronic structure problems, with no restriction except for the size of the systems or the defined multi-reference space. Because of the intrinsic multiconfigurational character of the problem, the combination of these procedures with the use of high-quality ANO basis sets and powerful algorithms for the determination of stationary points on the potential energy hypersurface has made MOLCAS the preferred package in the field of excited state quantum chemistry.[165] In the 90s, the accuracy of CASSCF and CASPT2 to deal with the excited states of small to medium size organic, inorganic, and organometallic molecules was established, and hundreds of spectroscopical problems were successfully solved.[54,94,166–172] More recently, the development of new methods such as MS (Multistate) CASPT2[13] or RASPT2[96] and the implementation of specifically constrained optimization procedures such as the calculation of Minimum Energy Paths (MEPs) or Minimum Energy Crossing Points (MECPs)[173] has expanded the applicability of the package to the field of non-adiabatic photophysics and photochemistry. In particular, CASSCF is still the only method generally applicable to deal with the degeneracy problem in the excited state (i.e., conical intersections, singlet-triplet crossings, high density of states, etc.), and MOLCAS is one of the few packages able to tackle those challenging problems efficiently. Obviously these capabilities extend its successful use to transition metal[174] or heavy-element[66] chemistry. A combined search of these terms (methods and topics) in recent literature yields no less than 600 entries.

Excited states are the actors of photochemical reactions induced by the absorption of light of appropriate wavelength. This process culminates in the formation of an electronically excited state of the molecule, which decays to lower energy states by means of nonradiative [e.g., internal conversions (IC), inter-system crossings (ISC) or energy transfer to other species] or radiative (e.g., fluorescence or phosphorescence) transitions. The energy is finally dissipated to the surroundings or used to yield new photoproducts. Figure 12 displays a scheme of the most important photophysical and photochemical molecular phenomena.[175] In an initial step,

[†]A patch applicable to the original TINKER sources and a simple manual (including some test cases) can be found at the URL: http://sites.univ-provence.fr/lcp-ct/ferre/nf_tinker_qmmm.html.

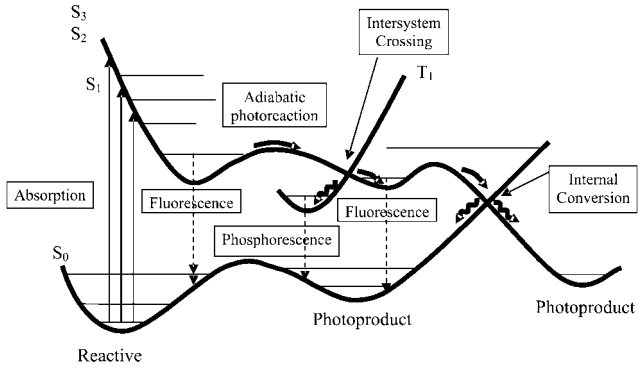

Figure 12. Scheme of the main photophysical and photochemical molecular events.

the description of such processes requires the accurate and balanced determination of the complex topology of potential energy hypersurfaces (PEHs) determining favorable reaction paths and state couplings. Further studies should include the dynamic (time-dependent and statistical) effects involved in the evolution of the system on the PEHs.

The CASPT2 method has shown to be feasible and adequate to deal with all types of electronic structure cases and PEHs, provide accurate energies and lead to conclusive results. Particularly difficult cases such as the simultaneous treatment of compact valence and diffuse Rydberg states[166,176] or close degeneracy situations[177] can also be properly treated with the MS-CASPT2 approach,[13] which provides orthogonal solutions for the states (unlike single-state CASPT2). As important as the energies are the matrix elements which inform about the probability of the energy transfer between the states, for absorption, emission, and radiationless decay. MOLCAS includes the CASSI/RASSI (CAS/RAS State Interaction) procedure,[23,24] a solid approach that yields all types of interaction matrix elements of the Hamiltonian and other operators over a wave function basis, including orthogonal or nonorthogonal states. It has been extensively used to compute transition dipole moments (and the corresponding oscillator strengths or radiative rates) and spin-orbit couplings.[65,178–183]

Understanding the spectroscopy and photochemistry of a molecular system means (at least from a static, topological viewpoint) to know large areas of the PEHs, including states minima, reaction paths, transition states, and state crossing regions. MOLCAS had previously efficient optimization algorithms to determine stationary points using simple or multiple geometrical constraints, and equally applicable to the ground and the excited states. Together with procedures based on analytical gradients at the CASSCF and RASSCF levels of calculation, for small systems it is possible to perform optimizations at higher levels such as CASPT2 or MS-CASPT2 using numerical gradients, even within a parallel computational framework. As long the procedures were used successfully, especially in electronic and vibrational spectroscopy, for instance to predict the existence of dark states in polyenes[184–186] or determine accurate vibrational band shapes.[168–171]

More recently new algorithms were implemented that, by including specific geometry or energy constraints, allow the determination of more particular structures. As an important tool, MOLCAS incorporates the calculation of Minimum Energy Paths (MEPs) as the lowest-energy reaction path followed by the system along a specific state. A MEP can be considered as the initial and most favorable path to describe the evolution of the energy along a state and the only one able to guarantee the presence or absence of energy barriers. In MOLCAS, they are built as steepest descent paths in a procedure[173] which is based on a modification of the Projected Constrained Optimization (PCO) algorithm of Anglada and Bofill[187] and follows the Müller-Brown approach.[188] Each step requires the minimization of the PEH on a hyperspherical cross section of the PEH centered on the initial geometry and characterized by a predefined radius. The optimized structure is taken as the center of a new hypersphere of the same radius, and the procedure is iterated until the bottom of the energy surface is reached. Mass-weighted coordinates are used, therefore the MEP coordinate corresponds to the so-called Intrinsic Reaction Coordinates (IRC). Figure 13 (top) displays an example of calculation in the 9H-guanine molecule.[189] Each point of the MEP is computed at the CASSCF level as the lowest-energy optimized structure in the target state (the spectroscopic $^1L_a\pi\pi^*$ of guanine) located at a distance from the original (Franck-Condon) geometry equal to the radius of an hypersphere centered in such initial structure. At each of the CASSCF MEP structures, a single-point CASPT2 calculation is performed. The outcome leads to predict the key photochemical event in the guanine molecule. Upon UV irradiation, in which the main spectroscopic state is populated in a major extent, the system evolves along the MEP in a barrierless way towards a region of crossing with the ground state. The major part of the absorbed energy is then efficiently dissipated in an ultrafast manner to the environment and an internal conversion takes place in which the population is finally switched to the ground state via a predicted CI $(gs/^1L_a)_{CI}$. This type of topology suggests that, as all other DNA nucleobase monomers,[190–193] guanine is highly photostable after UV absorption.

Another important tool allows to perform a structural optimization constrained to maintain a given energy difference (degeneracy, in general) between two selected states. In this manner, a general Minimum Energy Crossing Point (MECP) search can be performed, yielding the lowest energy point fulfilling the energy difference restriction. The search is performed using a restricted Lagrange multipliers technique.[173] If the MECP is defined between states of different multiplicities, the exact topological feature has been found, that is, the lowest energy point belonging to the hyperplane (seam) of structures responsible for a nonradiative ISC process. Analyzing the probability of ISC requires first to determine the accessibility of the ISC crossing point. A good strategy is to compute a MEP in the initially populated state (typically a singlet in most systems), and from the MEP points to find how accessible can the ISC crossing region be. It might occur that the MEP is barrierless toward such region[178,179] or that some barrier has to be surmounted.[180] MOLCAS allows tracing the corresponding path by combining the MEP and MECP algorithms, that is optimizing MECP structures at controlled distances and directions from a given geometry. This procedure may lead to MEPs going upward, for instance defined in a space perpendicular to a specific vector (e.g., the main path direction).[173] Other possibility is to compute a transition state and define a photoadiabatic reaction (see Fig. 12).[191–193] As an illustration Figure 14 displays a number of seams of minimum (SOM) energy points computed to analyze the photochemistry of acrolein,[173]

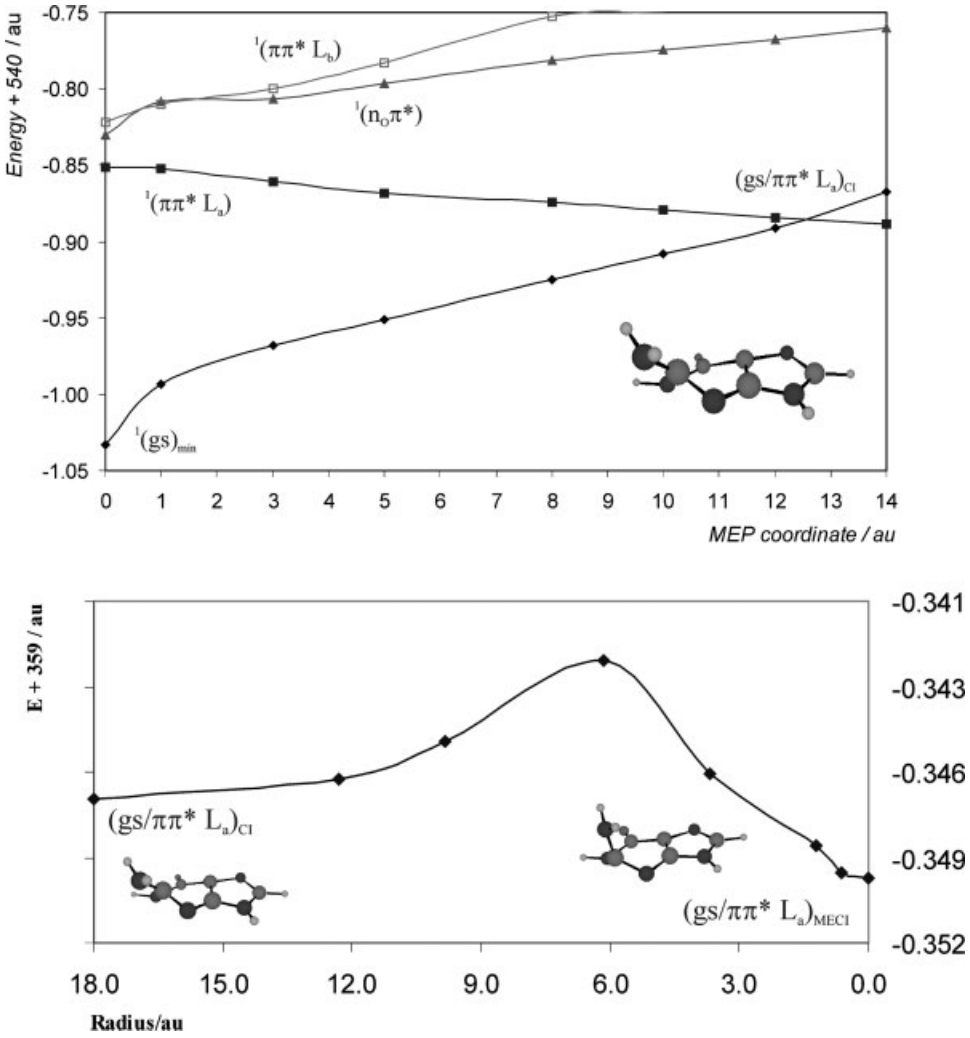

Figure 13. Computed CASPT2//CASSCF MEP (top) for the decay of the lowest $\pi\pi^*$ state of 9H-guanine and CASSCF seam (bottom) of degeneracy points from the Minimal Energy Crossing Point (MECI) toward the crossing at the end of the MEP (CI).

finding the Near Crossing Point (NCP) from a given structure by mapping the seam space. Populating the final state (triplet in general) requires the combined effects of a small energy-gap (state crossing region) and large spin-orbit coupling terms, whose magnitude (controlling the ISC transfer probability) can be accounted for with the RASSI program, which can compute matrix elements over spin-orbit states.[24,178–183] Recently De Vico and Lindh[194] have demonstrated an excellent alternative to the SOM approach. They applied a combination of several constraints, i.e., degeneracy plus hypersphere search plus the orthogonality condition, to search for various seams perpendicular to a MEP. This did not only establish a one-to-one map between a MEP and one or several seams, but also demonstrated which molecular vibrations populate the individual seams.

It is known that most of the photochemistry takes place, however, via IC between states of the same multiplicity, and the main topological protagonists of the energy transfer process are the regions of conical intersections (CI). Topologically, the structures belonging to an hyperline or seam of CIs fulfill the degeneracy condition along all coordinates except two, the states gradient difference and the Non-adiabatic Coupling Elements (NACMEs) between the interacting states, terms which are discarded in the usual Born-Oppenheimer framework. In MOLCAS-7 the calculation of NACMEs is not ready yet and therefore the state crossing algorithm yields strictly MECP, not Minimum Energy Conical Intersections (MECI). In practice, however, the structural difference between both features is not large, as observed in different cases.[189] Figure 13 (bottom) illustrates the use of MOLCAS to solve a problem involving CIs. Once determined in guanine the MEP controlling the evolution of the spectroscopic singlet excited state from the Franck-Condon region and leading in a barrierless way toward a degeneracy region with the ground state,[189] it is possible to determine the MECI (actually MECP) supposedly responsible of the IC process, in this case displaying (bottom of the drawing) an almost 90° out-of-plane distortion of the NH_2 group in guanine.[189] The assumption that the MECI is the most relevant structure that must be reached to trigger the IC process is common in

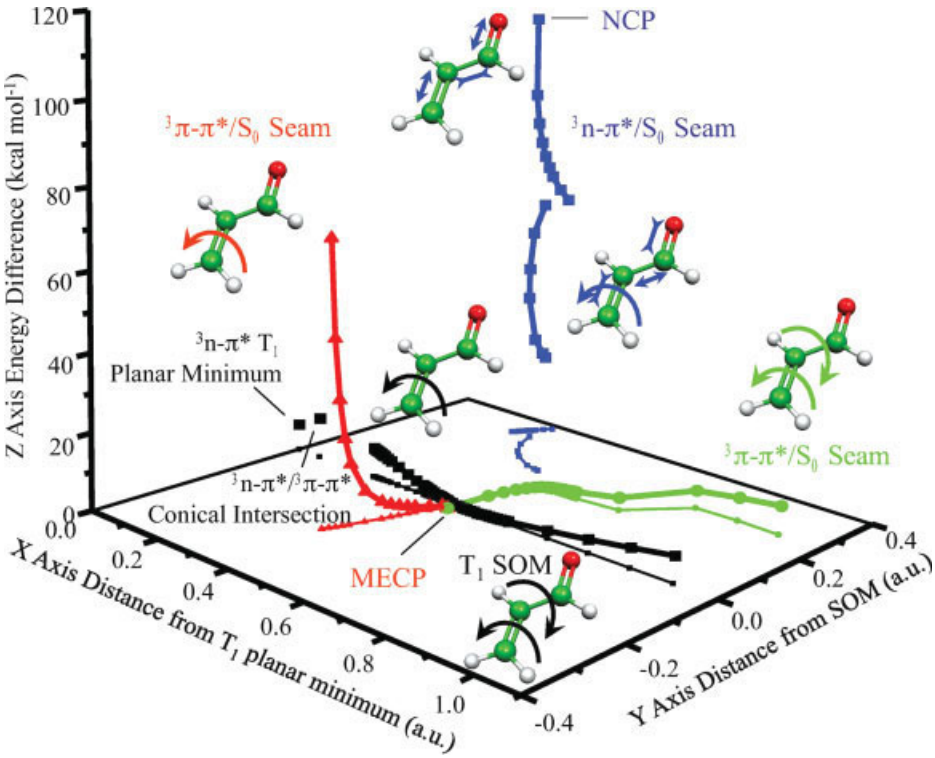

Figure 14. Computed paths and seams in acrolein. (By permission of American Chemical Society).

the literature, but incorrect. The most relevant CI (or seam of CIs) is not the lowest-energy CI (or MECI) but the most accessible one. In the case of guanine it was proved that the seam of CIs extends from the MECI region toward the end of the MEP, in which the degeneracy seam is easily accessible, whereas an energy barrier prevents the MECI to be reached. Tracing the seam of CIs is possible by combining two restrictions in a constrained optimization of the molecule in its excited state: degeneracy between the first and second singlet states and distance from the reference geometry (MECI here) at successive radius of the hypersphere. Each individual optimization generates one point of the seam (see Fig. 13) until the region of the end of the MEP was reached and the really significant CI described.

Non-adiabatic photochemistry is a new and emergent field for theoretical chemistry, where many recent methods and algorithms have to be incorporated to the codes and where a number of limitations are still present in the calculations. Due to the size of the problems most of the photochemical studies use the CASPT2//CASSCF computational strategy, that is, geometries and energies determined at the CASSCF and CASPT2 levels, respectively. In most cases, the results are accurate enough, although one has to be aware of the problems with differential correlation, that is, the correlation energy may affect differently to the states, and, for instance, two degenerate states in a CASSCF MECP may dramatically split at the CASPT2 or MS-CASPT2 levels.[175,177] The problems can be generally solved in small systems performing CASPT2 or MS-CASPT2 geometry determinations[195,196] using numerical gradients. It is expected that MOLCAS incorporates in the near future important tools such as analytical CASPT2 gradients, NACME elements to characterize CIs, and even procedures to get trajectories for semiclassical reaction dynamics.[189,197] Together with the available procedures to mimic environmental effects (continuum models, QM/MM, embedding potentials),[26,163,198–200] they will extend the applicability of the package in the future in the field of photochemistry.

Summary

The most recent version of MOLCAS, version 7, has been updated, as compared with earlier versions, with respect to methods and implementations which should facilitate calculations of much larger molecular systems and/or correlating more electrons. These improvements encompass methods to handle larger basis sets via a general tool, based on the Cholesky decomposition, to generate auxiliary basis functions either explicitly or implicitly. This approach has been generalized to be applicable to the HF, pure and hybrid DFT, MP2, CCSD, CCSD(T), CASSCF, RASSCF, CASPT2, MS-CASPT2, and RASPT2 wave function models. The article presents the theory and techniques behind these improvements and numerous examples are provided to demonstrate the capacity of these new developments. Especially, the improvements with respect coupled-cluster theory and the RASPT2 methods are presented in some details. With these new developments the MOLCAS package supports highly correlated calculations (CASPT2 and CC) in excess of 1000 basis functions. Furthermore, the

MOLCAS package has been improved with respect to the applicability of the one-component wave functions models to address chemical problems involving elements of the whole periodic table. In particular, the paper demonstrates the benefits of the so-called ANO-RCC basis set library covering all elements and presents the theory and implementation of the picture-change-free property integrals to be used in association with relativistic calculations originating from the DKH transformation. The ESPF QM/MM interface, the MOLCAS/TINKER implementation, which in principle can handle any kind of MM forcefield, is presented and discussed. The manuscript is concluded with a section, which in some details, describes the usefulness of the MOLCAS package in association with the study of photochemistry. More specifically, the implementation of constrained geometry optimization to facilitate the search for MEPs, MECPs, ISCs, and CIs are discussed as well as the analysis of the relationship between reaction paths and seams of various nature. This section is supported by illustrative examples.

Acknowledgments

N.F. thanks M. Olivucci for the figure illustrating the QM/MM section.

References

1. Lindh, R.; Malmqvist, P.-Å. Theor Chem Acc 2003, 110, 115.
2. Roos, B. Chem Phys Lett 1972, 15, 153.
3. Siegbahn, P. E. M. In Current Aspects of Quantum Chemistry 1981: Proceedings of an International Conference and Workshop, Barcelona, Spain, 28 September – 3 October 1981; Carbó, R., Ed.; Elsevier Scientific Publishing Company: Amsterdam, 1987; p 65.
4. Roos, B. O.; Taylor, P. R.; Siegbahn, P. E. M. Chem Phys 1980, 48, 157.
5. Siegbahn, P. E. M.; Almlöf, J.; Heiberg, J.; Roos, B. O. J Chem Phys 1981, 74, 2384.
6. Roos, B. O. Int J Quantum Chem 1980, S14, 175.
7. Roos, B.; Veillard, A.; Vinot, G. Theor Chim Acta 1971, 20, 1.
8. Roos, B.; Siegbahn, P. Theor Chim Acta 1970, 17, 209.
9. Roos, B.; Siegbahn, P. Theor Chim Acta 1970, 17, 199.
10. Andersson, K.; Malmqvist, P.-Å.; Roos, B. O.; Sadlej, A. J.; Wolinski, K. J Phys Chem 1990, 94, 5483.
11. Andersson, K.; Malmqvist, P.-Å.; Roos, B. O. J Chem Phys 1992, 96, 1218.
12. Andersson, K.; Roos, B. O. In Modern Electron Structure Theory Advanced Series in Physical Chemistry, Vol. 2, Part I; Yarkony, R., Ed.; World Scientific Publishing Co. Pte. Ltd.: Singapore, 1995; pp. 55.
13. Finley, J.; Malmqvist, P.-Å.; Roos, B. O.; Serrano-Andrés, L. Chem Phys Lett 1998, 288, 299.
14. Lindh, R.; Ryu, U.; Liu, B. J Chem Phys 1991, 95, 5889.
15. Ryu, U.; Lee, Y. S.; Lindh, R. Chem Phys Lett 1991, 185, 562.
16. Lindh, R. Theor Chim Acta 1993, 85, 423.
17. Stålring, J.; Bernhardsson, A.; Lindh, R. Mol Phys 2001, 99, 103.
18. Lindh, R.; Bernhardsson, A.; Karlström, G.; Malmqvist, P.-Å. Chem Phys Lett 1995, 241, 423.
19. Lindh, R.; Bernhardsson, A.; Schütz, M. Chem Phys Lett 1999, 303, 567.
20. Bernhardsson, A.; Lindh, R.; Olsen, J.; Fülscher, M. Mol Phys 1999, 96, 617.
21. Olsen, J.; Roos, B. O.; Jørgensen, P.; Jensen, H. J. A. J Chem Phys 1988, 89, 2185.
22. Malmqvist, P.-Å.; Rendell, A.; Roos, B. O. J Phys Chem 1990, 94, 5477.
23. Malmqvist, P. Å.; Roos, B. O. Chem Phys Lett 1989, 155, 189.
24. Malmqvist, P.-Å.; Roos, B. O.; Schimmelpfennig, B. Chem Phys Lett 2002, 357, 230.
25. Neogrády, P.; Pitoňák, M.; Urban, M. Mol Phys 2005, 103, 2141.
26. Karlström, G.; Lindh, R.; Malmqvist, P.-Å.; Roos, B. O.; Ryde, U.; Veryazov, V.; Widmark, P.-O.; Cossi, M.; Schimmelpfennig, B.; Neogrády, P.; Seijo, L. Comput Mater Sci 2003, 28, 222.
27. Veryazov, V.; Widmark, P.-O.; Serrano-Andrés, L.; Lindh, R.; Roos, B. O. Int J Quantum Chem 2004, 100, 626.
28. Benoit, C. E. Bull Geodesique 1924, 7, 67.
29. Golub, G. H.; Van Loan, C. F. Matrix Computations, 3rd Edition; Johns Hopkins University Press: Baltimore, 1996.
30. Beebe, N. H. F.; Linderberg, J. Int J Quantum Chem 1977, 12, 683.
31. Koch, H.; Sánchez de Merás, A.; Pedersen, T. B. J Chem Phys 2003, 118, 9481.
32. Pedersen, T. B.; Sánchez de Merás, A. M. J.; Koch, H. J Chem Phys 2004, 120, 8887.
33. Whitten, J. L. J Chem Phys 1973, 58, 4496.
34. Baerends, E. J.; Ellis, D. E.; Ros, P. Chem Phys 1973, 2, 41.
35. Dunlap, B. I.; Connolly, J. W. D.; Sabin, J. R. J Chem Phys 1979, 71, 3396.
36. Dunlap, B. I.; Connolly, J. W. D.; Sabin, J. R. J Chem Phys 1979, 71, 4993.
37. Feyereisen, M.; Fitzgerald, G.; Komornicki, A. Chem Phys 1993, 208, 359.
38. Vahtras, O.; Almlöf, J.; Feyereisen, M. W. Chem Phys Lett 1993, 213, 514.
39. Aquilante, F.; Lindh, R.; Pedersen, T. B. J Chem Phys 2007, 127, 114107.
40. Aquilante, F.; Pedersen, T. B.; Sánchez de Merás, A.; Koch, H. J Chem Phys 2006, 125, Art. No 174101.
41. Aquilante, F.; Pedersen, T. B.; Lindh, R. J Chem Phys 2007, 126, Art. No 194106.
42. Aquilante, F.; Pedersen, T. B. Chem Phys Lett 2007, 449, 354.
43. Aquilante, F.; Lindh, R.; Pedersen, T. B. J Chem Phys 2008, 129, Art. No 034106.
44. Aquilante, F.; Pedersen, T. B.; Roos, B. O.; Sánchez de Merás, A.; Koch, H. J Chem Phys 2008, 129, Art. No 024113.
45. Aquilante, F.; Malmqvist, P.-Å.; Pedersen, T. B.; Ghosh, A.; Roos, B. O. J Chem Theory Comput 2008, 4, 694.
46. Aquilante, F.; Gagliardi, L.; Pedersen, T. B.; Lindh, R. J Chem Phys 2009, 130, 154107.
47. Boström, J.; Aquilante, F.; Pedersen, T. B.; Lindh, R. J Chem Theory Comput 2009, in press. DOI:10.1021/ct9000284.
48. Pierloot, K.; Vancoillie, S. J Chem Phys 2008, 128, Art. No 034104.
49. Radon, M.; Pierloot, K. J Phys Chem A 2008, 112, 11824.
50. Widmark, P.-O.; Malmqvist, P.-Å.; Roos, B. O. Theor Chim Acta 1990, 77, 291.
51. Widmark, P.-O.; Persson, B. J.; Roos, B. O. Theor Chim Acta 1991, 79, 419.
52. Pou-Amérigo, R.; Merchán, M. Nebot-Gil, I.; Widmark, P.-O.; Roos, B. O. Theor Chim Acta 1995, 92, 149.
53. Pierloot, K.; Dumez, B.; Widmark, P.-O.; Roos, B. O. Theor Chim Acta 1995, 90, 87.
54. Roos, B. O.; Andersson, K.; Fülscher, M. P.; Malmqvist, P.-Å.; Serrano-Andrés, L.; Pierloot, K.; Merchán, M. In Advances in Chemical Physics: New Methods in Computational Quantum Mechanics; Prigogine, I.; Rice, S. A., Eds.; Vol. XCIII:219–331, Wiley: New York, 1996; p. 219.
55. Roos, B. O.; Veryazov, V.; Widmark, P.-O. Theor Chem Acc 2004, 111, 345.

56. Roos, B. O.; Lindh, R.; Malmqvist, P.-Å.; Veryazov, V.; Widmark, P.-O. J Phys Chem A 2004, 108, 2851.
57. Roos, B. O.; Lindh, R.; Malmqvist, P.-Å.; Veryazov, V.; Widmark, P.-O. J Phys Chem A 2005, 109, 6575.
58. Roos, B. O.; Lindh, R.; Malmqvist, P.-Å.; Veryazov, V.; Widmark, P.-O. Chem Phys Lett 2005, 409, 295.
59. Roos, B. O.; Lindh, R.; Malmqvist, P.-Å.; Veryazov, V.; Widmark, P.-O.; Borin, A. C. J Phys Chem A 2008, 112, 11431.
60. Faegri K., Jr. Theor Chem Acc 2001, 105, 252.
61. Sansonetti, J.; Martin, W.; Young, S. Handbook of Basic Atomic Spectroscopic Data (version 1.00); [Online] Available at: http://physics.nist.gov/Handbook; National Institute of Standards and Technology: Gaithersburg, MD, 2003.
62. Lide D. R., Ed. Handbook of Chemistry and Physics; CRC Press: Boca Raton, 2002.
63. Reiher, M.; Wolf, A. Relativistic Quantum Chemistry; Wiley-VCH: Weinheim, 2009.
64. Roos, B. O.; Malmqvist, P.-Å.; Gagliardi, L. In Fundamental World of Quantum Chemistry; Brändas, E.; Kryachko, E., Eds.; Kluwer Acad. Publ.: Dordrecht, The Netherlands, 2003; p. 425.
65. Roos, B. O.; Malmqvist, P.-Å. Adv Quantum Chem 2004, 47, 37.
66. Gagliardi, L.; Roos, B. O. Chem Soc Rev 2007, 36, 893.
67. Douglas, M.; Kroll, N. M. Ann Phys 1974, 82, 89.
68. Hess, B. A. Phys Rev A 1986, 33, 3742.
69. Reiher, M.; Wolf, A. J Chem Phys 2004, 121, 2037.
70. Wolf, A.; Reiher, M.; Hess, B. A. J Chem Phys 2002, 117, 9215.
71. Reiher, M.; Wolf, A. Phys Lett A 2007, 360, 603.
72. Reiher, M.; Wolf, A. J Chem Phys 2004, 121, 10945.
73. Reiher, M. Theor Chem Acc 2006, 116, 241.
74. Baerends, E. J.; Schwarz, W. H. E.; Schwerdtfeger, P.; Snijders, J. G. J Phys B 1990, 23, 3225.
75. Kellö, V.; Sadlej, A. J. Int J Quantum Chem 1998, 68, 159.
76. Wolf, A.; Reiher, M. J Chem Phys 2006, 124, Art. No 064102.
77. Wolf, A.; Reiher, M. J Chem Phys 2006, 124, Art No 064103.
78. Mastalerz, R.; Barone, G.; Lindh, R.; Reiher, M. J Chem Phys 2007, 127, Art. No 074105.
79. Luber, S.; Ondík, I. M.; Reiher, M. Chem Phys 2009, 356, 205.
80. Mastalerz, R.; Lindh, R.; Reiher, M. Chem Phys Lett 2008, 465, 157.
81. Barone, G.; Mastalerz, R.; Lindh, R.; Reiher, M. J Phys Chem A 2008, 112, 1666.
82. Chan, G. K.-L.; Dorando, J. J.; Gosh, D.; Hachmann, J.; Neuscamman, E.; Wang, H.; Yanai, T. In Frontiers in Quantum Systems in Chemistry and Physics, Vol. 18; Wilson, S.; Grout, P. J.; Maruani, J.; Delgado-Barrio, G.; Piecuch, P., Eds.; Springer: Dordrecht, Netherlands, 2008; p. 49.
83. Marti, K. H.; Ondík, I. M.; Moritz, G.; Reiher, M. J Chem Phys 2008, 128, Art. No. 014104.
84. Ghosh, D.; Hachmann, J.; Yanai, T.; Chan, G. K.-L. J Chem Phys 2008, 128, Art. No. 144117.
85. Celani, P.; Stoll, H.; Werner, H.; Knowles, P. Mol Phys 2004, 102, 2369.
86. Angeli, C.; Pastore, M.; Cimiraglia, R. Theor Chim Acta 2007, 117, 743.
87. Gagliardi, L.; Roos, B. O. Nature 2005, 433, 848.
88. Gagliardi, L.; Heaven, M. C.; Krogh, J. W.; Roos, B. O. J Am Chem Soc 2005, 127, 86.
89. Gagliardi, L.; Pyykkö, P.; Roos, B. O. Phys Chem Chem Phys 2005, 7, 2415.
90. Gagliardi, L.; Roos, B. O. In Trends and Perspectives in Modern Computational Science (ICCMSE06); Maroulis, G.; Simos T., Eds.; Brill Academic Publishers: The Netherlands, 2006; Ch. 2, p. 23.
91. LaMacchia, G.; Brynda, G. M.; Gagliardi, L. Angew Chem Int Ed Eng 2006, 45, 6210.
92. Roos, B. O.; Gagliardi, L. Inorg Chem 2006, 45, 803.
93. Ghosh, A.; Gonzalez, E.; Tangen, E.; Roos, B. O. J Phys Chem A 2008, 112, 12792.
94. Schreiber, M.; Silva, M. R., Jr.; Sauer, S. P. A.; Thiel, W. J Chem Phys 2008, 128, Art. No 134110.
95. Celani, P.; Werner, H.-J. J Chem Phys 2000, 112, 5546.
96. Malmqvist, P.-Å.; Pierloot, K.; Shahi, A. R. M.; Cramer, C. J.; Gagliardi, L. J Chem Phys 2008, 128, Art. No 204109.
97. Čížek, J. J Chem Phys 1966, 45, 4256.
98. Paldus, J.; Li, X. Z. Adv Chem Phys 1999, 110, 1.
99. Bartlett, R. J. In Advanced Series in Physical Chemistry, Vol. 2; Yarkony, D. R., Ed.; World Scientific: Singapore, 1995; p. 1047.
100. Urban, M.; Černušák, I.; Noga, J.; Kellö, V. In Methods in Computational Chemistry, Vol. 1; Wilson, S., Ed.; Plenum Press: New York, 1987; p. 117.
101. Gauss, J.; Schleyer, P. v. R., Ed. Encyclopedia of Computational Chemistry; Wiley: Chichester, 1998; p. 615.
102. Bartlett, R. J.; Musial, M.; Rev Mod Phys 2007, 79, 291.
103. Li, X. Z.; Paldus, J. J Chem Phys 1997, 107, 6257.
104. Pittner, J.; Šmydke, J.; Čársky, P.; Hubač, I. Theochem-J Mol Struct 2001, 547, 239.
105. Musial, M.; Kucharski, S. A.; Bartlett, R. J. J Chem Phys 2002, 116, 4382.
106. Piecuch, P.; Kucharski, S. A.; Bartlett, R. J. J Chem Phys 1999, 110, 6103.
107. Chattopadhyay, S.; Pahari, D.; Mukherjee, D.; Mahapatra, U. S. J Chem Phys 2004, 120, 5968.
108. Raghavachari, K.; Trucks, G. W.; Pople, J. A.; Head-Gordon, M. Chem Phys Lett 1989, 157, 479.
109. Urban, M.; Noga, J.; Cole, S. J.; Bartlett, R. J. J Chem Phys 1985, 83, 4041.
110. Noga, J.; Bartlett, R. J. J Chem Phys 1987, 86, 7041.
111. Noga, J.; Bartlett, R. J.; Urban, M. Chem Phys Lett 1987, 134, 126.
112. Li, X. Z.; Paldus, J. J Chem Phys 1994, 101, 8812.
113. Kallay, M.; Surjan, P. R. J Chem Phys 2001, 115, 2945.
114. Neogrády, P.; Szalay, P. G.; Kraemer, W. P.; Urban, M. Collect Czech Chem Commun 2005, 70, 951.
115. Stanton, J. F.; Gauss, J.; Watts, J. D.; Bartlett, R. J. J Chem Phys 1991, 94, 4334.
116. Urban, M.; Neogrády, P.; Hubač, I. In Recent Advances in Computational Chemistry, Vol. 3; Bartlett, R. J., Ed.; World Scientific: Singapore, 1997; p. 275.
117. Neogrády, P.; Urban, M. Int J Quantum Chem 1995, 55, 187.
118. Watts, J. D.; Gauss, J.; Bartlett, R. J. J Chem Phys 1993, 98, 8718.
119. Takahashi, M.; Paldus, J. J Chem Phys 1986, 85, 1486.
120. Heckert, M.; Heun, O.; Gauss, J.; Szalay, P. G. J Chem Phys 2006, 124, Art No 124105.
121. Koch, H.; deMeras, A. S.; Helgaker, T.; Christiansen, O. J Chem Phys 1996, 104, 4157.
122. Noga, J.; Valiron, P. Mol Phys 2005, 103, 2123.
123. Constans, P.; Ayala, P. Y.; Scuseria, G. E. J Chem Phys 2000, 113, 10451.
124. Olson, R. M.; Bentz, J. L.; Kendall, R. A.; Schmidt, M. W.; Gordon, M. S. J Chem Theory Comput 2007, 3, 1312.
125. Janowski, T.; Ford, A. R.; Pulay, P. J Chem Theory Comput 2007, 3, 1368.
126. Janowski, T.; Pulay, P. J Chem Theory Comput 2008, 4, 1585.
127. Lotrich, V.; Flocke, N.; Ponton, M.; Yau, A. D.; Perera, A.; Deumens, E.; Bartlett, R. J. J Chem Phys 2008, 128, Art. No 194104.
128. Koch, H.; de Meras, A. S. J Chem Phys 2000, 113, 508.
129. Constans, P.; Scuseria, G. E. Collect Czech Chem Commun 2003, 68, 357.
130. Maslen, P. E.; Dutoi, A. D.; Lee, M. S.; Shao, Y. H.; Head-Gordon, M. Mol Phys 2005, 103, 425.
131. Adamowicz, L.; Bartlett, R. J. J Chem Phys 1987, 86, 6314.

132. Adamowicz, L.; Bartlett, R. J.; Sadlej, A. J. J Chem Phys 1988, 88, 5749.
133. Pitoňák, M.; Neogrády, P.; Kellö, V.; Urban, M. Mol Phys 2006, 104, 2277.
134. Dedíková, P.; Pitoňák, M.; Neogrády, P.; Řezáč, I.; Urban, M. J Phys Chem A 2008, 112, 7115.
135. Šulka, M.; Pitoňák, M.; Neogrády, P.; Urban, M. Int J Quantum Chem 2008, 108, 2159.
136. Boman, L.; Koch, H. Int J Quantum Chem 2009, 109, 708.
137. Taube, A. G.; Bartlett, R. J. Collect Czech Chem Commun 2005, 70, 837.
138. Taube, A. G.; Bartlett, R. J. J Chem Phys 2008, 128, Art. No 164101.
139. Noga, J.; Kutzelnigg, W. J Chem Phys 1994, 101, 7738.
140. Laidig, W. D.; Purvis, G. D.; Bartlett, R. J. J Phys Chem 1985, 89, 2161.
141. Schütz, M.; Werner, H. J. J Chem Phys 2001, 114, 661.
142. Korona, T.; Pflüger, K.; Werner, H. J. Phys Chem Chem Phys 2004, 6, 2059.
143. Pitoňák, M.; Neogrády, P.; Řezáč, J.; Jurečka, P.; Urban, M.; Hobza, P. J Chem Theory Comput 2008, 4, 1829.
144. Pitoňák, M.; Riley, K. E.; Neogrády, P.; Hobza, P. Chem Phys Chem 2008, 9, 1636.
145. Dunning, T. H.; Peterson, K. A.; Woon, D. E. In Encyclopedia of Computational Chemistry; Schleyer, P. v. R., Ed.; Wiley: Chichester, 1998; p. 88.
146. Neogrády, P.; Medveď, M.; Černušák, I.; Urban, M. Mol Phys 2002, 100, 541.
147. Ervin, K. M.; Anusiewicz, I.; Skurski, P.; Simons, J.; Lineberger, W. C. J Phys Chem A 2003, 107, 8521.
148. González-Luque, R.; Merchán, M.; Fülscher, M. P.; Roos, B. O. Chem Phys Lett 1993, 204, 323.
149. Bachorz, R. A.; Klopper, W.; Gutowski, M. J Chem Phys 2007, 126, Art. No 085101.
150. Bachorz, R. A.; Klopper, W.; Gutowski, M.; Li, X.; Bowen, K. H. J Chem Phys 2007, 129, Art. No 054309.
151. Roca-Sanjuan, D.; Merchán, M.; Serrano-Andrés, L.; Rubio, M. J Chem Phys 2008, 129, Art No 095104.
152. Karlström, G. J Phys Chem 1988, 92, 1315.
153. Cossi, M.; Rega, N.; Scalmani, G.; Barone, V. J Chem Phys 2001, 114, 5691.
154. Barandiarán, Z.; Seijo, L. J Chem Phys 1988, 89, 5739.
155. Warshel, A.; Levitt, M. J Mol Biol 1976, 103, 227.
156. Field, M. J.; Bash, P. A.; Karplus, M. J Comp Chem 1990, 11, 700.
157. Lin, H.; Truhlar, D. G. Theor Chem Acc 2006, 117, 185.
158. Ferré, N.; Ángyán, J. G. Chem Phys Lett 2002, 356, 331.
159. Ponder, J. W. Tinker4.2—software tools for molecular design; Available at: http://dasher.wustl.edu/tinker; 2004.
160. Vreven, T.; Morokuma, K.; Farkas, O.; Schlegel, H. B.; Frisch, M. J. J Comput Chem 2003, 24, 760.
161. Coto, P. B.; Strambi, A.; Ferré, N.; Olivucci, M. Proc Natl Acad Sci USA 2006, 103, 17154.
162. Frutos, L. M.; Andruniów, T.; Santoro, F.; Ferré, N.; Olivucci, M. Proc Natl Acad Sci USA 2007, 104, 7764.
163. Strambi, A.; Coto, P. B.; Frutos, L. M.; Ferré, N.; Olivucci, M. J Am Chem Soc 2008, 130, 3382.
164. Roca-Sanjuán, D.; Olaso-González, G.; Rubio, M.; Brana-Coto, P.; Merchán, M.; Ferré, N.; Ludwig, V.; Serrano-Andrés, L. Pure Appl Chem 2009, 81, 743.
165. Olivucci, M., Ed. Computational Photochemistry; Elsevier: Amsterdam, 2005.
166. Roos, B. O.; Fülscher, M. P.; Malmqvist, P.-Å.; Merchán, M.; Serrano-Andrés, L. In Quantum Mechanical Electronic Structure Calculations with Chemical Accuracy; Langhoff, S. R., Ed.; Kluwer Academic Publishers, Understanding Chem. React.: Dordrecht, The Netherlands, 1995; p. 357.
167. Merchán, M.; Serrano-Andrés, L.; Fülscher, M. P.; Roos, B. O. In Recent Advances in Multireference Theory, Vol. IV; K. H. U., Ed.; World Scientific Publishing Co, Pte. Ltd: Singapore, 1999; p. 161.
168. Serrano-Andrés, L.; Forsberg, N.; Malmqvist, P.-Å. J Chem Phys 1998, 108, 7202.
169. Bernhardsson, A.; Forsberg, N.; Malmqvist, P.-Å.; Roos, B. O.; Serrano-Andrés, L. J Chem Phys 2000, 112, 2798.
170. Pou-Amérigo, R.; Serrano-Andrés, L.; Merchán, M.; Ortí, E.; Forsberg, N. J Am Chem Soc 2000, 122, 6067.
171. Roos, B. O.; Malmqvist, P.-Å.; Molina, V.; Serrano-Andrés, L.; Merchán, M. J Chem Phys 2002, 116, 7526.
172. Serrano-Andrés, L.; Merchán, M. Chem Phys Lett 2006, 418, 569.
173. De Vico, L.; Lindh, R.; Olivucci, M. J Chem Theory Comput 2005, 1, 1029.
174. Pierloot, K. Mol Phys 2003, 101, 2083.
175. Serrano-Andrés, L.; Merchán, M. J Mol Struct Theochem 2005, 729, 99.
176. Pérez-Hernández, G.; González, L.; Serrano-Andrés, L. Chem Phys Chem 2008, 9, 2544.
177. Serrano-Andrés, L.; Merchán, M.; Lindh, R. J Chem Phys 2005, 122, Art. No 104106.
178. Climent, T.; González-Luque, R.; Merchán, M.; Serrano-Andrés, L. Chem Phys Lett 2007, 441, 327.
179. Serrano-Pérez, J. J.; González-Luque, R.; Merchán, M.; Serrano-Andrés, L. J Phys Chem B 2007, 111, 11880.
180. Merchán, M.; Serrano-Andrés, L.; Robb, M. A.; Blancafort, L. J Am Chem Soc 2005, 127, 1820.
181. Climent, T.; González-Luque, R.; Merchán, M.; Serrano-Andrés, L. J Phys Chem A 2006, 110, 13584.
182. Serrano-Pérez, J. J.; Serrano-Andrés, L.; Merchán, M. J Chem Phys 2006, 124, Art. No 124502.
183. Liu, Y.-J.; De Vico, L.; Lindh, R.; Fang, W.-H. Chem Phys Chem 2007, 8, 890.
184. Serrano-Andrés, L.; Sánchez-Marín, J.; Nebot-Gil, I. J Chem Phys 1992, 97, 7499.
185. Serrano-Andrés, L.; Merchán, M.; Nebot-Gil, I.; Lindh, R.; Roos, B. O. J Chem Phys 1993, 98, 3151.
186. Serrano-Andrés, L.; Lindh, R.; Roos, B. O.; Merchán, M. J Phys Chem 1993, 97, 9360.
187. Anglada, J. M. Bofill, J. M. J Comput Chem 1997, 18, 992.
188. Müller, K.; Brown, L. D.; Theor Chim Acta 1979, 53, 75.
189. Serrano-Andrés, L.; Merchán, M.; Borin, A. C. J Am Chem Soc 2008, 130, 2473.
190. Merchán, M.; González-Luque, R.; Climent, T.; Serrano-Andrés, L.; Rodríguez, E.; Reguero, M.; Peláez, D. J Phys Chem B 2006, 110, 26471.
191. Serrano-Andrés, L.; Merchán, M.; Borin, A. C. Proc Natl Acad Sci USA 2006, 103, 8691.
192. Serrano-Andrés, L.; Merchán, M.; Borin, A. C. Chem Eur J 2006, 12, 6559.
193. Serrano-Andrés, L.; Merchán, M. J Photochem Photobiol C (in press).
194. De Vico, L.; Lindh, R. J Chem Theory Comput 2009, 5, 186.
195. De Vico, L.; Wisborg-Krogh, J.; Liu, Y.-J.; Lindh, R. J Phys Chem A 2007, 111, 8013.
196. De Vico, L.; Pegado L.; Heimdal, J.; Söderhjelm, P.; Roos, B. O. Chem Phys Lett 2008, 461, 136.
197. Weingart, O.; Shapiro, I.; Buss, V. J Phys Chem B 2007, 111, 3782.
198. Serrano-Andrés, L.; Fülscher, M. P.; Karlström, G. Int J Quantum Chem 1997, 65, 167.
199. Proppe, B.; Merchán, M.; Serrano-Andrés, L. J Phys Chem A 2000, 104, 1608.
200. Seijo, L.; Barandiarán, Z. In Computational Chemistry: Reviews of Current Trends, Vol. 4; Leszczynski, J., Ed.; World Scientific: Singapur; 1999; p. 55.